Climatically driven biogeographic provinces of Late Triassic tropical Pangea

Jessica H. Whiteside[a,1], Danielle S. Grogan[a], Paul E. Olsen[b,1], and Dennis V. Kent[b,c]

[a]Department of Geological Sciences, Brown University, 324 Brook Street, Box 1846, Providence, RI 02912; [b]Lamont-Doherty Earth Observatory, Columbia University, 61 Route 9W, Palisades, NY 10964; and [c]Department of Earth and Planetary Sciences, Rutgers University, Piscataway, NJ 08854

Contributed by Paul E. Olsen, March 3, 2011 (sent for review January 17, 2011)

Although continents were coalesced into the single landmass Pangea, Late Triassic terrestrial tetrapod assemblages are surprisingly provincial. In eastern North America, we show that assemblages dominated by traversodont cynodonts are restricted to a humid 6° equatorial swath that persisted for over 20 million years characterized by "semiprecessional" (approximately 10,000-y) climatic fluctuations reflected in stable carbon isotopes and sedimentary facies in lacustrine strata. More arid regions from 5–20°N preserve procolophonid-dominated faunal assemblages associated with a much stronger expression of approximately 20,000-y climatic cycles. In the absence of geographic barriers, we hypothesize that these variations in the climatic expression of astronomical forcing produced latitudinal climatic zones that sorted terrestrial vertebrate taxa, perhaps by excretory physiology, into distinct biogeographic provinces tracking latitude, not geographic position, as the proto-North American plate translated northward. Although the early Mesozoic is usually assumed to be characterized by globally distributed land animal communities due to of a lack of geographic barriers, strong provinciality was actually the norm, and nearly global communities were present only after times of massive ecological disruptions.

biotic provinciality | Cynodontia | orbital forcing | Procolophonidae | latitudinal gradient

Geographic and climatic barriers are among the main constraints on the distribution of organisms. During the Late Triassic, Pangea lacked significant geographic barriers nearly pole-to-pole, and was warm and equable without glaciation or sea ice (1). Nonetheless, when correlated temporally by nonbiostratigraphic means, diverse Late Triassic continental faunal and floral assemblages display dramatic differences across paleolatitude (e.g., refs. 2–4) (Fig. 1). Although the equator-to-pole temperature gradients may have been relatively weak, Milankovitch-type climatic variability expressed in precipitation and evaporation was nonetheless very important (5–8). Then, as now (9,10), this scale of temporal variability may have played a critical role in structuring terrestrial communities, and thus early Mesozoic sequences provide a unique window into the link between climate variability and biotic provinciality.

Here, we focus on the tropical regions of Late Triassic central Pangea and the role of traversodont cynodonts (basal synapsids) and procolophonids (parareptiles) as possible ecologically equivalent herbivores (Fig. 2) under different climatic regimes. We test the correlation between climate variability and biotic provinces within narrow swaths of time constrained by astrochronology, paleomagnetic polarity stratigraphy, and paleomagnetically determined plate position from long [>5 million years (My)] lacustrine and associated fluvial records spanning 30° of paleolatitude. We show that faunal composition tracks different modes of orbitally forced climate variability that maintained Pangean faunal provinces and suggest that this may be a common feature of continental ecosystems.

Geologic, Climatic, and Biotic Context

Exposed eastern North America rift basins, formed during the incipient breakup of Pangea, comprise a northeast-southwest transect across the paleo-equator and tropics (Fig. 1). Best known is the Newark basin that, during the approximately 32 My. covered by its continuously cored record (11, 12), translated northward with central Pangea, transecting zonal climate belts from the equator to 20°N (8, 13, 14). The astrochronologic and paleomagnetic polarity constraints on this sequence allow tight temporal calibration and correlation to other basin sections in eastern North America (Fig. 1). Perhaps because of the extreme continentality of the climate of Pangea or elevated temperatures associated with high atmospheric CO_2 concentrations (15, 16), these lacustrine records were extremely sensitive to insolation changes driven by celestial mechanics (6, 7, 17) as exemplified by the tropical (5–20°N) Newark basin lacustrine record displaying lake-level cycles with periods of approximately 20 thousand years (ky) (precession), approximately 100 ky (short eccentricity), and 405 ky (long eccentricity) (6). This record also reveals longer periods of climatic precession modulation of approximately 1.8 My and approximately 3.5 My cycles (7), but it notably lacks convincing obliquity periods (6), indicating that precession and eccentricity controlled lake-level cyclicity at these latitudes.

To examine the links between the expression of cyclical climate mode and biotic provinciality, we analyzed cores and measured outcrop sections in seven eastern North American rift basins from Nova Scotia to South Carolina, which together with the 20° of northward translation of the Newark basin extend the latitudinal transect an additional 5° south and 5° north, spanning a total of 30° of latitude (Fig. 1).

Many terrestrial vertebrates have been found in these rift basin sequences, including rich assemblages of hitherto unexpected composition (18). Most surprising are assemblages containing abundant small (skull length, 3–10 cm) traversodont cynodonts from multiple localities and levels within the Richmond and Deep River basins (Figs. 1 and 2) (e.g., refs. 18–20). Such assemblages were previously known exclusively from Gondwana (e.g., refs. 21, 22), and are still unknown from the American Southwest (23). Coeval strata from other eastern North America basins have produced assemblages of more familiar aspect, where procolophonid parareptiles of similar size to the cynodonts are abundant (24, 25). In these strata, traversodont cynodonts are either absent or very rare.

Traversodont cynodonts and procolophonids have dentitions that display at least superficially similar specializations for herbivory (25–27), consistent with a diet of tough, fibrous plant material (28, 29) (Fig. 2). Their mutually exclusive abundance patterns

Author contributions: J.H.W. designed research; J.H.W., D.S.G., P.E.O., and D.V.K. performed research; J.H.W. contributed new reagents/analytic tools; J.H.W., D.S.G., P.E.O., and D.V.K. analyzed data; and J.H.W. wrote the paper.

The authors declare no conflict of interest.

[1]To whom correspondence may be addressed. E-mail: Jessica_Whiteside@Brown.edu or polsen@ldeo.columbia.edu.

This article contains supporting information online at www.pnas.org/lookup/suppl/doi:10.1073/pnas.1102473108/-/DCSupplemental.

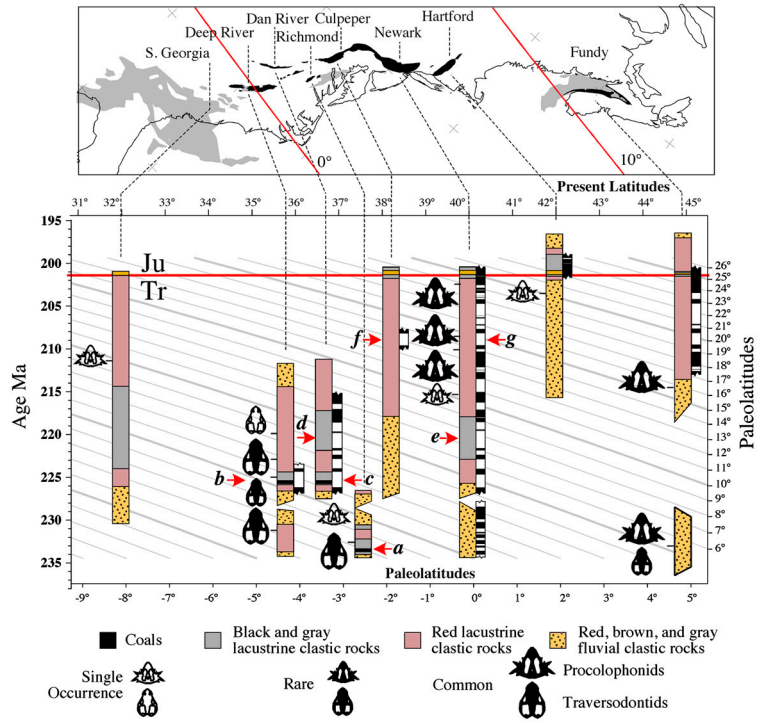

Fig. 1. (*Upper*) Map of basins studied. (*Lower*) Time-geography nomogram showing correlation of key rift basin sections in eastern North America, typical facies, and distribution of traversodonts and procolophonids. Time scale and paleolatitudes are based on the Newark basin section (6–8, 30). The gray curved lines are lines of equal paleolatitude assuming rift basins are within a rigid plate and all drift with Pangea. Red arrows show the position of the studied sections (*SI Text*): (*A*) Vinita Formation; (*B*) Cumnock Formation; (*C*) lower member Cow Branch Formation; (*D*) upper member Cow Branch Formation; (*E*) Lockatong Formation; (*F*) Balls Bluff Formation; (*G*) Passaic Formation.

and similar trophic adaptations suggest they could be ecological equivalents. Paleomagnetic polarity correlations (8, 11, 30, 31) and occurrences from multiple levels within several of these basins demonstrate that these disparate assemblages are broadly coeval, and that the traversodont-dominated assemblages occur in strata deposited within a few degrees of the equator, whereas procolophonid-dominated assemblages are found in higher tropical to subtropical latitudes. Thus, the differences between the assemblages suggest strong biotic provinciality, on a continent where an ambitious tetrapod could theoretically have walked from the Triassic location of Sydney to Vladivostok.

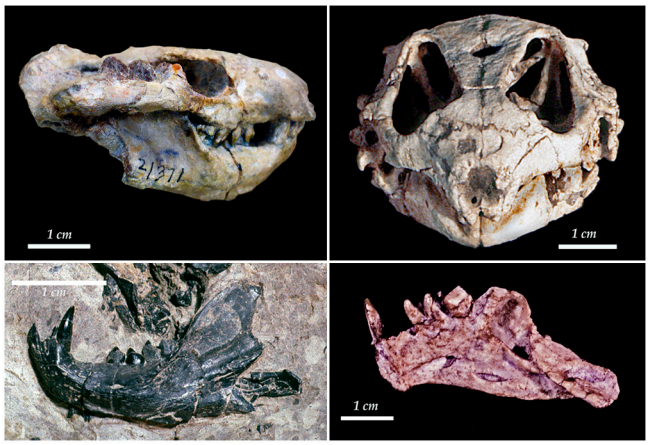

Fig. 2. Examples of traversodont cynodonts from equatorial latitudes (*Left*) and procolophonoid parareptiles from higher tropical latududes (*Right*). Skull is above, and mandible showing teeth is below. Scale bar, 1 cm. See *SI Text* for specimen data.

Core and Outcrop Materials

We analyzed lacustrine time series of environmental proxies from five basins and six lacustrine formations that collectively span a paleolatitudinal range of 17° and a temporal interval of 25 My (Figs. 1 and 3) from 209 to 234 Ma. Core and outcrop metadata are given in *SI Text* with ages based on the Newark basin astronomically tuned geomagnetic polarity time scale (Newark-APTS) correlation (32) (see *SI Text*). The environmental proxies used in our analyses are primarily related to lake depth and related ecosystem function (see *Methods*) that are in turn related to climate-driven water balance fluctuations. These include depth ranks (facies indicating different degrees of lake depth or desiccation), color (related to the redox state and organic carbon content of the sediment), total organic carbon (TOC—related to the redox state of the environment), and $\delta^{13}C_{toc}$ [related to the differential preservation of organic matter with different stable carbon isotopic ratios (33)].

Tropical Precessional Forcing

The records we examined were deposited in lakes in the tropics, and it is important to examine our expectations of orbitally forced water balance variability. Exactly what component of orbital forcing is important to water balance in the tropics is debatable (see ref. 34), but there is a growing consensus that the intensity of insolation drives the intensity of convection and hence precipitation in tropical monsoonal systems (34). Because the calendar date of the time of maximum precipitation is not constant, normal orbital solutions fixed to a date do not capture a time series of the intensity of maximum insolation.

In the tropics, the sun passes directly overhead both at the vernal and autumnal equinoxes, causing two warm and often two wet seasons. The position of the equinoxes with respect to perihelion gradually shifts over time, causing the two warm seasons to alternately coincide with annual maximum insolation (Fig. 4) (35). This coincidence occurs twice every precessional

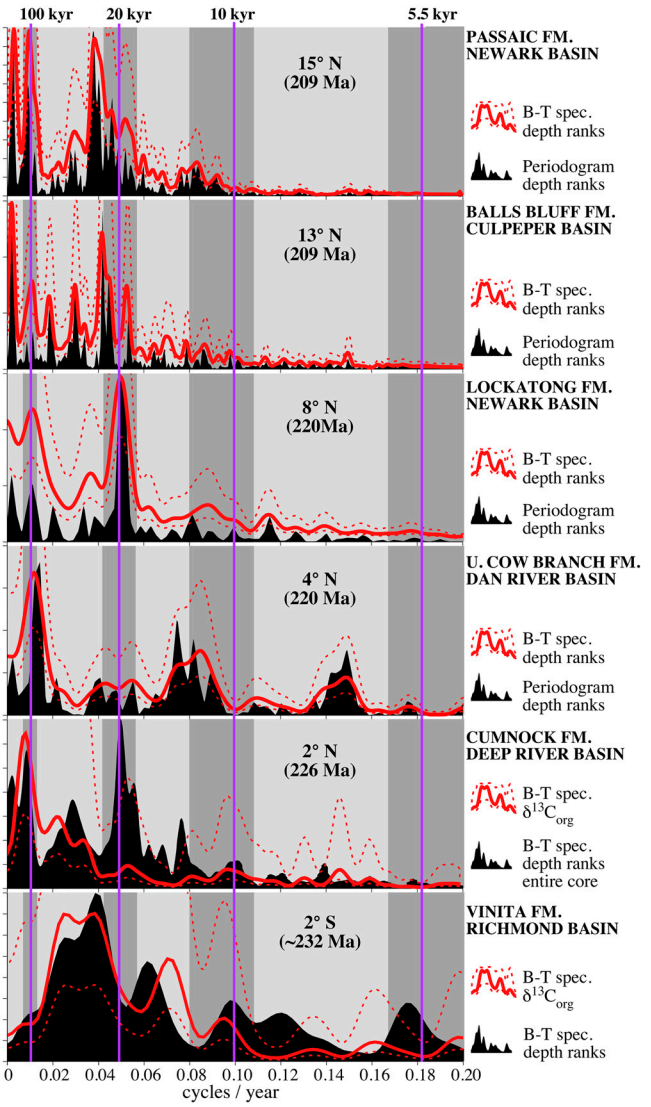

Fig. 3. Frequency spectra of the lacustrine sections. Measured sections and data curves of depth ranks, color, $\delta^{13}C_{org}$, and TOC are given in the *SI Text*. Darker gray bands show the range of frequencies expected for specific periods (purple).

cycle, resulting in an approximately 10-ky cycle (actually 9–12 ky) in tropical annual maximum insolation (Fig. 4) (35–37). Because at the tropics of Cancer and Capricorn the sun is directly overhead only once a year, the time of maximum insolation independent of the calendar date (Fig. 4) forms a clear latitudinally dependent pattern. At the equator, an approximately 10 ky cycle is present as well as a relative amplification of the spectral expression of the eccentricity cycles because of the asymmetry caused by "rectification" of the precession cycles induced in the insolation curve (36). This approximately 10-ky cycle is of precessional origin but has half-precessional periods, and it is termed semiprecession. Proceeding from the equator, the amplitude of the approximately 10-ky cycle and the eccentricity cycles decrease, whereas that of the familiar approximately 20-ky cycle increases, until the ~20-ky cyclicity dominates at the tropics and the ~10-ky cycle is absent (38). In as much as precipitation is coupled to convergence, lake high stands should be coupled to the period of maximum insolation. Therefore, in a monsoonal system we expect to see an approximately 10-ky cycle in lake depth within a few degrees of the equator.

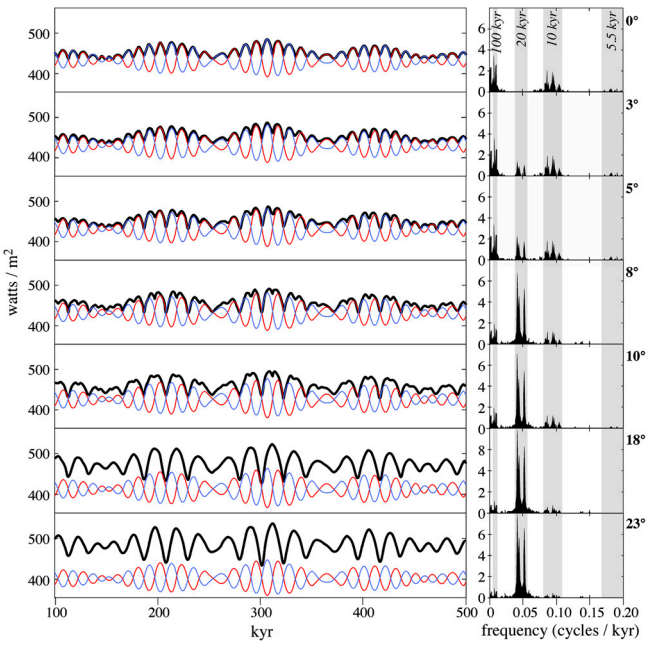

Fig. 4. (*Left*) Magnitude of maximum insolation (black), insolation at the vernal equinox (blue), and insolation at the autumnal equinox (red) from the equator to 23°N based on the La2004 solution (see *Methods*). (*Right*) Frequency spectra of maximum insolation showing the prevalent semiprecessional peak at frequency 0.10 near the equator, and the strong obliquity peak at frequency 0.05 farther north.

Energy balance models (36) and atmospheric general circulation models (34, 39, 40) capture this semiprecessional cycle in temperature and consequent precipitation variations, and both continental and marine Quaternary tropical climate records reveal at least a component of semiprecessional forcing (41–45). Increased temperature gradients caused by large northern hemisphere land masses enhance both the intensity and regional extent of precessional influences on hydrology in general circulation models (34), and therefore precessional and semiprecessional forcing of tropical hydrologic variations may have been enhanced during the Triassic existence of Pangea.

Spectral Results

The Richmond, Deep River, and Dan River basins' lacustrine records (Fig. 1) display periodicities consistent with orbital forcing within the available age model constraints including cycles of roughly 405-, 100-, and 20-ky period in all of the proxy records (Fig. 3), as do the Newark and Culpeper basins. However, the former three basins also contain strong approximately 10-ky to approximately 15-ky semiprecessional cycles. This semiprecessional cycle is stronger than the approximately 20-ky cycle in the Cow Branch Formation in the Dan River Basin, which is the equatorial section with the best temporal correlation to the Newark-APTS (see *SI Text* for details).

Our proxy time series tend to be highly asymmetrical, resembling a clipped precessional signal (see *SI Text*). Although power spectra of clipped precession signals can display artifactual semiprecession frequencies as result of the clipping itself, this is not the case in these data, because visual inspection shows peaks in the time series of the proxy data at the expected half cycle position, most apparent in direct comparison between the contemporaneous equatorial upper member of the Cow Branch Formation (4° N) and higher latitude Lockatong Formation (8°) (see *SI Text*). Other datasets show the same pattern as well, such as the taxonomic composition of palynomorph assemblages and organic matter type as seen in the Vinita Formation (46, 47). Thus, at the same time approximately 20-ky cycles dominated

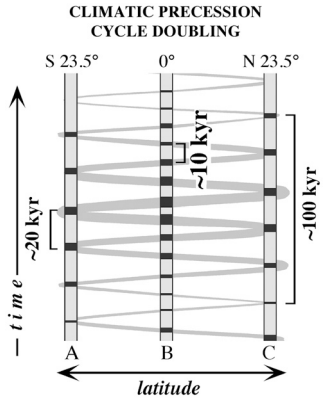

Fig. 5. Conceptual model showing relationship between the latitude of the coincidence of perihelion and the solstice through time. Width of the sinusoidal line is proportional to the insolation intensity at the coincidence of perihelion and solstice following the eccentricity cycles. *A*, *B*, and *C* represent hypothetical lacustrine sections showing lithological variations caused by lake level cycles produced by changes in precipitation tracking the yearly insolation maximum. *A* and *C* have pure approximately 20-ky cycles, whereas *B* at the equator has only an approximately 10-ky cycle.

the climate of the Newark basin region, approximately 10-ky cycles were dominant 4° to the south in the Dan River basin as predicted by local insolation forcing (Fig. 4) and our conceptual model (Fig. 5).

Discussion

The geographic pattern of periodicities seen in these Late Triassic rift basins corroborate the hypothesis that local forcing of climate, largely through the maximum intensity in insolation, independent of calendar date, controlled lake depth. The sections in the eastern North America Triassic rift basins with different modes of climate variability also have different faunas. The equatorial sections with relatively well-developed semiprecessional variability are dominated by traversondont cynodonts. But the sections deposited in higher tropical and subtropical latitudes not only show much weaker (or no) approximately 10-ky cyclicity, but also have different vertebrate assemblages characterized by abundant procolophonids, whereas traversodont cynodonts are virtually absent. A striking example is the higher paleolatitude (approximately 6°N), 233-Ma middle Wolfville Formation assemblage of the Fundy Basin. Abundant and diverse procolophonids occur in these fluvial strata and include the genera *Scoloparia*, *Acadiella*, and *Haligonia* (24). The only traversodont cynodont present is the rare and comparatively huge *Arctotraversodon* (dentary length = 40 cm) (ref. 48; H-D Sues, personal communication, 2010). Conversely, in the low paleolatitude Pekin (approximately 3°S) and Vinita (approximately 4°) formations, procolophonids are very rare, represented only by two specimens (49), among hundreds of specimens of the traversodont cynodont *Boreogomphodon* (50).

It is worth emphasizing that the approximately 10-ky cyclicity occurs at independently determined equatorial paleolatitudes where coals are preserved (5), along with the traversodont cynodonts. It is likely that the coupling of the double rainy season that is linked to the approximately 10-ky cyclicity with more intense equatorial insolation was responsible for the greater mean humidity and less intense dry periods of the region, which favored the traversodont cynodonts and coal formation. Support for this hypothesis that humidity was critical comes from Gondwanan high latitudes, where Late Triassic assemblages with abundant traversodont cynodonts also occur (4, 51). These specifically include the Ischigualastian assemblages of Argentina and the Santa Maria assemblages of Brazil associated with abundant gray, plant-bearing strata (52). Apparently, traversodont cynodonts had very disjunct ranges during the Late Triassic and were largely limited to humid zones. The distinct, apparently climate-related, provinciality of the Late Triassic is associated with high diversity globally, in dramatic contrast to the Early Jurassic in which global faunas are evidently homogenized, at least at higher taxonomic levels (2).

At a larger scale, floral data also shows a strong pattern of latitude-related provinciality, with time-transgressive microfloral assemblages being characteristic of low to higher latitudinal sedimentary basin successions (32) resulting from the northward translation of central Pangea, paralleling the pattern observed in larger vertebrates (2). Because the ranges of pollen and spores is often used for long range biostratigraphic correlation, there has been a strong tendency to conflate these biogeographic patterns with a biostratigraphic (i.e., temporal) signal in the absence, or even in the face of, strong, biostratigraphically independent means of temporal correlation (e.g., ref. 53).

The documentation of latitudinal separation of distinct vertebrate biotic provinces is consistent with the suggestion that Late Triassic archosaurs also show latitudinal differences (2, 4, 54, 55). These data show clear differences between taxa from the tropical semiarid zone of the American Southwest in comparison to the more humid high-latitude assemblages of South America. Astronomically forced latitudinal climate differences predict these observed differences and may indicate they were a major driver of Late Triassic terrestrial biogeography. More specifically, they also explain a long-standing puzzling pattern: the lack of traversodont cynodonts from fossiliferous strata in the American Southwest that were deposited north of the equatorial belt (13).

One possible mechanism limiting abundant traversodont cynodonts to equatorial and temperate latitudes might be their nitrogen excretion physiology. Synapsids, including humans and traversodonts, are ureotelic and retain the primitive tetrapod condition in which excreted urea is diluted by abundant water (56). In contrast, nearly all living sauropsids are uricotelic synthesizing uric acid (56), a feature likely present in procolophonids (see *SI Text*). The water used in synthesizing uric acid is recovered when it is precipitated prior to excretion, and hence, living sauropsids (including lizards and birds) tend to have an advantage over living synapsids—mammals—in water-poor areas. Thus, if procolophonids had sauropsid uricotely, they would be expected to be more successful at surviving water stress encountered not only seasonally, but more severely during the megadroughts at times of maximum precessional variability approximately every 20-ky cycle at extraequatorial tropical and subtropical latitudes. These arid intervals would be less extreme in the zone dominated by approximately 10-ky cyclicity. Because physiological water balance strategies are highly conserved among sauropsid and synapsid clades, this would be a likely mechanism to allow climate to sort the abundance of members of these clades, especially during extreme climate events.

Conclusions

Late Triassic equatorial Pangea lake levels followed an approximately 10-ky and approximately 20-ky cyclicity attributable to the control of precipitation by the doubling of the frequency of the climatic precession cycle. Contemporaneous lacustrine records from the higher latitude Newark basin show much less effect of the approximately 10-ky cycle and a correspondingly stronger ~20-ky cycle of "normal" climatic precession. The dominance of the ~20-ky cycle of climatic precession increased in younger strata as central Pangea drifted north during the Late Triassic (13). Biotic provinciality tracks the modes of climate variability with traversodont cynodont-dominated assemblages present in areas with ~10-ky cyclicity, whereas procolophonids are dominant in regions with the more familiar ~20-ky cyclicity. Even in a time of low equator-to-pole gradients, no ice, and no geographic barriers, Milankovitch variability, and climate in general, appears sufficient to have produced strong biotic provinciality. Physiological constraints acted on by climate extremes during times of high precessional variance may have been a key ecological structuring

mechanisms. Biotic provinciality driven by zonal climate belts coupled with ecological incumbency, priority, or niche preemption effects (e.g., ref. 57) that develop as a consequence of the basic climatic structure may be prevalent when geographic barriers are minimal except at times of extreme ecological reorganization, such as the end-Permian (2, 58), and end-Triassic mass extinctions (2, 16) and the Paleocene-Eocene Thermal Maximum (59, 60) hyperthermal.

Methods

Depth Rank and Color. Depth rank, a proxy of relative lake depth, is a classification of facies by suites of sedimentary structures in which facies are assigned a value of 0 to 5 in order of increasing relative water depth (7, 17). Color is related to the reduction-oxidation state of the sedimentary environment.

Carbon Isotopic Analyses. From each section of interest, we took samples at submeter intervals for bulk carbon isotopic ($\delta^{13}C_{org}$) and TOC analyses. Samples were weighed into methanol-rinsed Ag boats, acidified in a desiccator over concentrated HCl for 72 h at 60–65 °C, dried for 24 h at 60–65 °C, and dried for an additional 24 h at 60–65 °C in a desiccator with silica gel. Samples were wrapped in Sn immediately prior to analysis. $\delta^{13}C_{org}$ and TOC measurements were made on a Costech 4010 Elemental Analyzer (EA) with a Zero-Blank carousel coupled to a Thermo DeltaVPlus stable light isotope ratio mass spectrometer (IRMS) at Brown University. Samples were flash-combusted in the EA at 1020 °C in a pure oxygen pulse, with resulting products being fully oxidized to CO_2 in a metal oxide bed, subsequent reduction of NO_x to N_2 in a copper bed, and chromatographic separation prior to admission to the IRMS. Standardization with reference pulses resulted in isotopic accuracy and precision better than 0.3% for CO_2.

Time Series Analysis. Time series analysis was performed using Analyseries 2.0.4.2 (61). The age models were developed either by direct correlation to the Newark-APTS by paleomagnetic polarity stratigraphy or by identification of one of the thickness periodicities as the 405-ky cycle of eccentricity (see *SI Text* for details).

Daily Insolation Model. For this model, daily solar insolation averaged over 24 h at latitude φ and day λ (rad, independent of calendar date) is given by (62, 63)

$$W = (S_0/\pi) \cdot [1 + e\cos(\lambda\text{-}\omega\text{-}\pi)]^2/(1-e^2)^2 \cdot (H_0 \sin\varphi \sin\delta + \cos\varphi \cos\delta \sin H_0), \quad [1]$$

where S_0 is the solar constant (1,365 W/m^2), H_0 is the hour angle, and δ is the declination angle. The orbital parameters of eccentricity e, obliquity ε, and precession ω are given by Laskar et al. (64) (abbreviated below as La2004) and provide

$$\sin\delta = \sin\varepsilon \sin\lambda \quad [2]$$

and

$$\cos H_0 = -\tan\varphi \tan\delta. \quad [3]$$

At the equator, maximum insolation occurs approximately at the equinoxes (vernal equinox, $\lambda = 0$; autumnal equinox, $\lambda = \pi$), and minimum insolation occurs approximately at the solstices (summer solstice, $\lambda = \pi/2$; winter solstice $\lambda = 3\pi/2$), although the exact values of maximum and minimum λ vary slightly over time (37). Moving away from the equator, maximum and minimum λ vary with increasing magnitude.

To find the magnitude and day of maximum and minimum insolation at latitude φ, we use a MATLAB program that implements Eq. **1** and the La2004 orbital parameter solution (SI Text). The program iteratively calculates daily solar insolation for $\lambda_{max} \pm$ d rad and $\lambda_{min} \pm$ d rad with steps of 0.02 rad, where λ_{max} and λ_{min} are the equinoxes and solstices, respectively. For $\varphi < 10°$, $d = 0.8$ is sufficient. For $\varphi > 10°$, d must increase with φ.

ACKNOWLEDGMENTS. We thank Carl Johnson for laboratory assistance. We are grateful to Sterling Nesbitt, Christine Janis, Bill Ryan, and two anonymous reviewers for helpful comments on earlier versions of this manuscript. We thank Robert J. Barron, Jack Boyland, Ted Daeschler, Andy Heckert, Vince Schneider, Joseph P. Smoot, and Hans-Dieter Sues for locality information. We thank the North Carolina and Virginia geological surveys for access to cores and permission to take samples. J.H.W. acknowledges support from the Richard Salomon Foundation and a National Science Foundation Advance award to Brown University, and P.E.O. is grateful for support from National Science Foundation Grant EAR 0753496.

1. Frakes LA, Francis JE, Syktus JL (1992) *Climate Modes of the Phanerozoic: The History of the Earth's Climate over the Past 600 Million Years* (Cambridge Univ Press, Cambridge, UK) p 274.
2. Shubin NH, Sues H-D (1991) Biogeography of early Mesozoic continental tetrapods: Patterns and implications. *Paleobiology* 17:214–230.
3. Olsen PE, Galton PM (1984) A review of the reptile and amphibian assemblages from the Stormberg of southern Africa, with special emphasis on the footprints and the age of the Stormberg. *Palaeontol Afr* 25:92–110.
4. Ezcurra MD (2010) Biogeographic analysis of Triassic tetrapods: Evidence for biotic provincialism and driven sympatric cladogenesis in the early evolution of modern tetrapod lineages. *Proc R Soc London Ser B* 277:2547–2552.
5. Olsen PE (1997) Stratigraphic record of the early Mesozoic breakup of Pangea in the Laurasia-Gondwana rift system. *Annu Rev Earth Planet Sci* 25:337–401.
6. Olsen PE, Kent DV (1996) Milankovitch climate forcing in the tropics of Pangea during the Late Triassic. *Palaeogeogr Palaeoclimatol Palaeoecol* 122:1–26.
7. Olsen PE, Kent DV (1999) Long-period Milankovitch cycles from the Late Triassic and Early Jurassic of eastern North America and their implications for the calibration of the early Mesozoic time scale and the long-term behavior of the planets. *Philos Trans R Soc A* 357:1761–1787.
8. Kent DV, Tauxe L (2005) Corrected Late Triassic latitudes for continents adjacent to the North Atlantic. *Science* 307:240–244.
9. Brown K, Ab'Sabar AH (1979) Ice age forest refuges and evolution in the Neotropics: Correlation of paleoclimatological, geomorphological, and pedological data with modern biological endemism. *Paleoclimas* 5:1–30.
10. Colinvaux PA, et al. (1996) A long pollen record from lowland Amazonia: Forest and cooling in glacial times. *Science* 276:85–88.
11. Kent DV, Olsen PE (1999) Astronomically tuned geomagnetic polarity time scale for the Late Triassic. *J Geophys Res* 104:12831–12841.
12. Kent DV, Olsen PE (2008) Early Jurassic magnetostratigraphy and paleolatitudes from the Hartford continental rift basin (eastern North America): Testing for polarity bias and abrupt polar wander in association with the central Atlantic magmatic province. *J Geophys Res* 113:B06105, 10.1029/2007JB005407.
13. Kent DV, Irving E (2010) Influence of inclination error in sedimentary rocks on the Triassic and Jurassic apparent pole wander path for North America and implications for Cordilleran tectonics. *J Geophys Res* 115:B10103, 10.1029/2009JB007205.
14. Kent DV, Olsen PE (2000) Magnetic polarity stratigraphy and paleolatitude of the Triassic-Jurassic Blomidon Formation in the Fundy basin (Canada): Implications for early Mesozoic tropical climate gradients. *Earth Planet Sci Lett* 179:311–324.
15. Schaller MF, Wright JD, Kent DV (2011) Atmospheric P_{CO_2} perturbations associated with the Central Atlantic Magmatic Province. *Science* 331:1404–1409.
16. McElwain JC, Beerling DJ, Woodward FI (1999) Fossil plants and global warming at the Triassic-Jurassic boundary. *Science* 285:1386–1390.
17. Olsen PE (1986) A 40-million-year lake record of early Mesozoic climatic forcing. *Science* 234:842–848.
18. Sues H-D, Olsen PE (1990) Triassic vertebrates of Gondwana aspect from the Richmond basin of Virginia. *Science* 249:1020–1023.
19. Olsen PE, Schneider V, Sues H-D, Peyer KM, Carter JG (2001) Biotic provinciality of the Late Triassic equatorial humid zone. *Geol Soc Am Abstracts with Programs* 33:A-27, Available at http://gsa.confex.com/gsa/2001SE/finalprogram/abstract_4541.htm.
20. Heckert AB, Schneider VP, Olsen PE, Mitchell JS (2009) Vertebrate diversity of the Upper Triassic Chatham Group, Deep River basin, central North Carolina. *Abstracts, Second Annual Meeting of the Southeastern Association of Vertebrate Paleontology* (Virginia Museum of Natural History, Martinsville, VA), p 8, Available at http://web.me.com/dooleyclan/SEAVP/SEAVP_files/Abstract%20book.pdf.
21. Sues H-D, Olsen PE, Carter JG (1999) A Late Triassic traversodont cynodont from the Newark Supergroup of North Carolina. *J Vertebr Paleontol* 19:351–354.
22. Romer AS (1966) *Vertebrate Paleontology* (University of Chicago Press, Chicago), 3rd Ed.
23. Irmis RB, Parker WG (2005) Unusual tetrapod teeth from the Upper Triassic Chinle Formation, Arizona, USA. *Can J Earth Sci* 42:1339–1345.
24. Sues H-D, Baird D (1998) Procolophonidae (Reptilia: Parareptilia) from the Upper Triassic Wolfville Formation of Nova Scotia, Canada. *J Vertebr Paleontol* 18:525–532.
25. Sues H-D, Olsen PE, Scott DM, Spencer PS (2000) Cranial osteology of *Hypsognathus fenneri*, a latest Triassic procolophonid reptile from the Newark Supergroup of eastern North America. *J Vertebr Paleontol* 20:275–284.
26. Gow CE (1977) Tooth function and succession in the Triassic reptile *Procolophon trigoniceps*. *Palaeontology* 20:695–704.
27. Carroll RL, Lindsay W (1985) Cranial anatomy of the primitive reptile *Procolophon*. *Can J Earth Sci* 22:1571–1587.
28. Crompton AW, Attridge J (1986) *The Beginning of the Age of Dinosaurs*, ed K Padian (Cambridge Univ Press, Cambridge, UK), pp 223–236.

29. Wing SL, Sues H-D (1992) *Terrestrial Ecosystems Through Time*, eds AK Behrensmeyer et al. (University of Chicago Press, Chicago), pp 327–360.
30. Kent DV, Olsen PE, Witte WK (1995) Late Triassic-Early Jurassic geomagnetic polarity and paleolatitudes from drill cores in the Newark rift basin (Eastern North America). *J Geophys Res* 100:14965–14998.
31. Kent DV, Olsen PE (1997) Magnetostratigraphy and paleopoles from the Late Triassic Dan River-Danville basin: Interbasin correlation of continental sediments and a test of the tectonic coherence of Newark rift basins in eastern North America. *Geol Soc Am Bull* 109:366–377.
32. Olsen PE, Kent DV, Whiteside JH (2011) Implications of the Newark Supergroup-based astrochronology and geomagnetic polarity time scale (Newark-APTS) for the tempo and mode of the early diversification of the Dinosauria. *Earth Environ Sci Trans R Soc Edinburgh*, (in press).
33. Whiteside JH, et al. (2011) Pangean great lake paleoecology on the cusp of the end-Triassic extinction. *Palaeogeogr Palaeoclimat Palaeoecol* 301:1–17.
34. Clement AC, Hall A, Broccoli AJ (2004) The importance of precessional signals in the tropical climate. *Clim Dynam* 22:327–341.
35. Berger A, Loutre MF, Mélice JL (2006) Equatorial insolation: From precession harmonics to eccentricity frequencies. *Clim Past*, 2 pp:131–136, Available at http://www.clim-past.net/2/131/2006/cp-2-131-2006.html.
36. Crowley TJ, Kim K-Y, Mengel JG, Short DA (1992) Modeling 100,000 year climate fluctuations in pre-Pleistocene series. *Science* 255:705–707.
37. Ashkenazy Y, Gildor H (2008) Timing and significance of maximum and minimum equatorial insolation. *Paleoceangraphy* 23:PA1206, 10.1029/2007PA001436.
38. Laepple T, Lohmann G (2009) Seasonal cycle as template for climate variability on astronomical timescales. *Paleoceanography* 24:PA4201, 10.1029/2008PA001674.
39. Liu Z, Harrison SP, Kutzbach J, Otto-Bliesner B (2004) Global monsoons in the mid- Holocene and oceanic feedback. *Clim Dynam* 22:157–182.
40. Kutzbach JE, Liu X, Liu Z, Chen G-S (2008) Simulation of the evolutionary response of global summer monsoons to orbital forcing over the past 280,000 years. *Clim Dynam* 30:567–579.
41. Lyons RP, et al. (2009) Scientific drilling in continental East Africa: The dominance of eccentricity modulated precession and half-precession on continental tropical climate. *Eos Trans Am Geophys Union* PP11B-1315.
42. Verschuren D, et al. (2009) Half-precessional dynamics of monsoon rainfall near the East African Equator. *Nature* 462:637–641.
43. Pokras EM, Mix AC (1987) Earth's precession cycle and Quaternary climatic change in tropical Africa. *Nature* 326:486–487.
44. Hinnov LA (2000) New perspectives on orbitally forced stratigraphy. *Annu Rev Earth Planet Sci* 28:419–475.
45. McIntyre A, Molfino B (1996) Forcing of Atlantic equatorial and subpolar millennial cycles by precession. *Science* 274:1867–1870.
46. Ediger VS (1986) Paleopalynological biostratigraphy, organic matter deposition and basin analysis of the Triassic-(?)Jurassic Richmond rift basin, Virginia USA. PhD dissertation (Pennsylvania State Univ, State College, PA), p 425.
47. Malinconico MAL (2002) Lacustrine organic sedimentation, organic metamorphism and thermal history of selected Early Mesozoic Newark Supergroup basins, Eastern USA. PhD thesis (Columbia Univ, New York), p 419.
48. Sues H-D, Hopson JA, Shubin NH (1992) Affinities of ?*Scalenodontoides plemmyridon* Hopson, 1984 (Synapsida: Cynodontia) from the Upper Triassic of Nova Scotia. *J Vertebr Paleontol* 12:168–171.
49. Sues H-D, Olsen PE (1993) A new procolophonid and a new tetrapod of uncertain, possibly procolophonian affinities from the upper Triassic of Virginia. *J Vertebr Paleontol* 13:282–286.
50. Sues H-D, Hopson JA (2010) Anatomy and phylogenetic relationships of *Boreogomphodon jeffersoni* (Cynodontia: Gomphodontia) from the Upper Triassic of Virginia. *J Vertebr Paleontol* 30:1202–1220.
51. Rogers RR, et al. (1993) The Ischigualasto tetrapod assemblage (Late Triassic, Argentina) and $^{40}Ar/^{39}Ar$ dating of dinosaur origins. *Science* 260:794–797.
52. Colombi CE, Parrish JT (2008) Late Triassic environmental evolution in southwestern Pangea: Plant taphonomy of the Ischigualasto Formation. *Palaios* 23:778–795.
53. Van Veen PM (1995) Time calibration of Triassic/Jurassic microfloral turnover, eastern North America—Comment. *Tectonophysics* 245:93–95.
54. Irmis RB, et al. (2007) A Late Triassic dinosauromorph assemblage from New Mexico and the rise of dinosaurs. *Science* 317:358–361.
55. Nesbitt SJ, et al. (2009) A complete skeleton of a Late Triassic saurischian and the early evolution of dinosaurs. *Science* 326:1530–1533.
56. Wright PA (1995) Nitrogen excretion: Three end products, many physiological roles. *J Exp Biol* 198:273–281.
57. Valentine JW, Jablonski D, Krug AZ, Roy K (2008) Incumbency, diversity, and latitudinal gradients. *Paleobiology* 34:169–178.
58. Huey RB, Ward PD (2005) Hypoxia, global warming, and terrestrial Late Permian extinctions. *Science* 308:398–401.
59. Zachos JC, et al. (2006) Extreme warming of mid-latitude coastal ocean during the Paleocene-Eocene Thermal Maximum: Inferences from TEX86 and isotope data. *Geology* 34:737–740.
60. Bowen GJ, et al. (2002) Mammalian dispersal at the Paleocene/Eocene boundary. *Science* 295:2062–2065.
61. Paillard D, Labeyrie L, Yiou P (1996) Macintosh program performs time-series analysis. *Eos Trans Am Geophys Union* 77:379.
62. Milankovitch M (1941) *Kanon der Erdbestrahlung und seine Andwendung auf das Eiszeitenproblem* (Royal Serbian Academy of Science, Belgrade).
63. Berger A (1978) Long-term variations of daily insolation and Quaternary climatic changes. *J Atmos Sci* 35:2362–2367.
64. Laskar J, et al. (2004) A long-term numerical solution for the insolation quantities of the Earth. *Astron Astrophys* 428:261–285.

Supporting Information

Whiteside et al. 10.1073/pnas.1102473108

SI Text

Age Models and Explanation of Spectra for Sections in Main Text Fig. 3, Vago no. 1, Vinita Formation, Richmond Basin. The upper Vinita Formation of the Richmond basin has produced the second-richest traversodont-dominated assemblage (1, 2) known from the Newark Supergroup. The Richmond basin section is coal-bearing, but unlike the Deep River basin, most of the preserved basin section is lacustrine, and the markedly cyclical portion of the section (the Vinita Formation) is older than the Cumnock Formation, approximately the same age as the Pekin Formation.

The Vinita Formation differs dramatically from most other formations of the eastern North American rifts in that much of the lacustrine section lacks signs of subaerial exposure, indicating that the lakes rarely dried out. The Vago no. 1 (Fig. S1) core from the middle part of the Vinita Formation lacks any evidence of subaerial exposure. The observed cyclicity consists of alternating intervals of black microlaminated mudstone and interbedded graded sandstones (turbidites) with intervals of less well laminated mudstone.

The exact position of the Vago no. 1 core (Table S1) within the Vinita Formation is uncertain, but based on its overall black shale lithologies in comparision with the industry wells drilled in the basin, especially the Horner no. 1 well (Fig. S2 and Table S1), it appears to come from the lower third of the Vinita Formation, in the Manakin Member of ref. 3.

The accumulation rate in the Horner no. 1 well in the Richmond basin (Table S1) can be used to constrain that in the Vago no. 1 core (Fig. S2). We performed Fourier analysis of the pollen data displayed in ref. 4 (Dataset S1, *A*). We normalized and then averaged the individual spectra of pollen counts to produce an average spectrum (Fig. S2). The scale of the largest cycle, with a period of 832 m (2,731 ft), is comparable to the 1.75 million year (My) cycle identified in the Newark basin astronomically tuned geomagnetic polarity time scale (Newark-APTS) (5, 6). If this is correct, the cycle with a period of around 178 m (585 ft) should be the 405 thousand year (ky) eccentricity period with a corresponding inferred accumulation rate of 0.440 m/ky (1.5 ft/ky).

Fourier analysis of depth ranks from the entire Vago no. 1 core (Fig. S1; Table S2; Dataset S1, *B*; and Fig. 3 of the main text) shows prominent frequencies with periods at 9.38 m (31 ft) and 203.2 m (667 ft). Assuming that the higher frequency is the 20-ky cycle of climatic precession, the 203.2-m period corresponds to the 405-ky cycle. The small peak at 38.1 m (125 ft) probably represents the approximately 100-ky cycle. The inferred accumulation rate of 0.469 m/ky is close to that derived from the Horner no. 1 core (0.440 m/ky).

We sampled an interval from 26.8 to 64.5 m (88.0 to 211.7 ft) in the Vago core for bulk organic carbon isotopic analysis (Dataset S1, *B* and Fig. S1). Sixty-four samples were recovered amounting to 1 sample/0.4 m or 1 sample/900 y based on our accumulation rate model. The overall pattern of the relationship between depth ranks, total organic carbon (TOC), and $\delta^{13}C_{org}$ is that more ^{13}C-enriched values tend to be present in the deep water units, and values more depleted in ^{13}C are present in the shallower water units, consistent with the pattern seen in the Lockatong Formation. However, Fourier analysis of this interval shows the same peaks as the depth rank data from the entire core, but also a prominent peak at around 4.5 m (15 ft). Based on setting the 9.3-m peak to 20 ky, this peak should be about 10 ky. This semiprecessional peak corresponds in the time domain to a return to higher depth ranks about half way through the 20-ky cycle. Malinconico (7) looked at this same interval using organic petrographic techniques and noted that the mudstones with higher depth ranks have more algal material, whereas the mudstones with more poorly developed laminations tend to lack algal material. The latter units in our analyses correspond to the deeper water phase of the semiprecessional cycle and tend to have values more enriched in ^{13}C than the microlaminated units, which are the deepest water phase of the 20-ky climatic precession cycle. Ediger (8) also identified a double cycle in organic petrology and reasoned that it corresponded to the combined effect of the 20-ky precession and 40-ky obliquity cycles. At that time there was no expectation that a 10-ky cycle should be present at equatorial latitudes, and it was not known that the Vinita Formation was deposited at the equator. The "double cyclicity" observed by Ediger (8) and Malinconico (7) is more parsimoniously explained as an expression of the 10-ky cyclicity caused by local forcing at the equator.

MO-C-2-81 Core, Cumnock Formation, Deep River Basin. The Deep River basin is the most southerly exposed Pangean rift in eastern North America. The three nominal subbasins (Durham, Sanford, and Wadesboro) contain important cyclical lacustrine strata. The best-known of the lacustrine units, the coal-bearing Cumnock Formation of the Sanford basin, is comprised of Milankovitch-forced cycles (9, 10) and is represented by a series of 30.5- to 152.4-m (100- to 500-ft) cores taken for hydrocarbon exploration during the 1980s.

The MO-C-2-81 core (Figs. S1 and S3 and Table S1) recovered nearly the entire Cumnock Formation, although only the upper portion of the core was suitable for $\delta^{13}C_{org}$ analysis because of an igneous sill at the core bottom. We took 104 samples amounting to a rate of 1 sample/0.3 m or 1 sample/1,500 y based on the age model described below. Fourier analysis of the color proxy data (Fig. 3 of the main text and Dataset S1, *B*) reveals that the most prominent frequencies in the core are at periods of 3.8 m (12.5 ft) and 4.3 m (14.0 ft), and at 24.3 m (79.8 ft) and 82.1 m (269.4 ft).

We constrained the accumulation rate of the MO-C-2-81 core by paleomagnetic correlation to the Newark-APTS (Dataset S1, *C*). Because of the sill at the bottom of MO-C2-81, this core could not be used for paleomagnetic analysis. The core MO-C-4-81 (Table S1 and Fig. S3) was selected instead for paleomagnetic analysis because it consists largely of red strata, whereas gray strata of the Cumnock tends not to produce interpretable paleomagnetic results. Correlation to MO-C-2-81 is based on cyclostratigraphy (Fig. S3). We took 49 2.5-cm-diameter plugs of MO-C-4-81 for paleomagnetic analysis following the sampling procedure and analytical methods described by Kent et al. (11) (processed by M. Et-Touhami and P.M. LeTourneau) (Dataset S1, *C*). Plugs were drilled perpendicular to the core axis (assumed vertical) and where bedding dips were discernable, in the down-dip direction to assist in the interpretation of polarity in these azimuthally unoriented cores. Vector endpoint diagrams of thermal demagnetization of the natural remanence in 10 or more steps to 575 °C for gray samples (expected to have a magnetite remanence carrier) and 675 °C for red samples (expected to have a hematite carrier) were used to interpret magnetization components and to infer the polarity of the characteristic magnetization as gauged with respect to a normal polarity overprint that is commonly present according to fully oriented outcrop samples. The polarities could not be determined for samples with scattered (mainly gray) or even univectorial demagnetization trajectories. In the case of MO-C-4-81, both normal and reverse polarities are present, comprising an upper reverse polarity zone and a lower

mainly normal polarity zone, with a thin but distinct reverse polarity interval toward the base (Fig. S3).

To gain greater stratigraphic scope, we also recovered 47 plugs from the Deep River basin core CH-C-1-81 (Dataset S1, *C*). This core intersects red beds at the bottom (nominal Peking Formation) and a significant thickness of Sanford Formation at the top. Both in terms of gross lithology and detailed cyclostratigraphy, CH-C-1-81 is much more similar to MO-C-2-81 than it is to MO-C-4-81. Again, both normal and reverse polarities were present and as predicted for a basinal core, compared to MO-C-481, a much larger proportion of gray strata with nearly the full extent of the Cumnock Formation being represented. A transition from predominately normal to reverse polarity is apparent in the middle of the formation. There is a normal fault near the bottom of the core, which unfortunately cuts out strata in the position of the small reverse interval in the lower part of MO-C-4-81. Another small reverse interval is present at the base of the core, however. Both of these polarity zones would have a duration less than 40 ky based on our assessments of the cyclicity and the independently derived accumulation rate.

There is a prominent diabase sill in the upper part of the Cumnock Formation in CH-C-1-81. This sill is of normal polarity, and the surrounding aureole is also of normal polarity, surrounded by strata of reverse polarity. We omit this normal polarity interval from the composite stratigraphy because it is clearly an overprint from the sill intrusion. Finally, at the top of the core there is a short but distinct interval of normal polarity. Because it is represented by only three closely spaced samples, we do not regard it as a likely candidate for the base of a major normal polarity zone.

The Cumnock Formation cores barely penetrate into underlying red strata, and having only two main polarity zones, a unique correlation is not possible. To capture greater stratigraphic context and to place the Cumnock cores into the Newark-APTS, we sampled the SO-C-2-81 core in the Dan River basin, which recovered the basal part of the lower member of the Cow Branch Formation (Fig. S3), with 60 2.5-cm plugs for paleomagnetic analysis. The detailed stratigraphy of the lower member of the Cow Branch Formation is nearly identical to that of the Cumnock Formation including the position of coal beds, despite the fact that the two sites are 145 km apart in separate basins. Fourier analysis of the upper 122 m (400 ft) of the SO-C-2-81 core shows a hierarchy of frequencies similar to that seen in the Cumnock Formation (Fig. S4 and Dataset S1, *B*), except that the spectrum is noisier and the accumulation rate is higher in the lower member of the Cow Branch Formation, compared to the Cumnock Formation. The ratios of the homologous thickness periods corresponding to the approximately 100-ky cycles in the Cumnock and lower Cow Branch (23.8 m/33.9 m) is 0.702.

Polarities could not be determined for most samples from the Lower Cow Branch member because the lithologies are gray to black and the samples usually alter during thermal demagnetization. The exceptions occur near the very base of the formation where red beds are intercalated with gray, in which case all determinable samples were of normal polarity. Normal polarities were also seen in the mostly red Pine Hall Formation in SO-C-2-81, consistent with a close correlation of the lower Cumnock Formation. Although only two polarity zones are present in the composite section, the lower member of the Cow Branch lies stratigraphically below the long polarity stratigraphy described by Kent and Olsen (12) and thus has a well-constrained correlation to the Newark-APTS. Based on placing the SO-C-2-81 core in context with the rest of the Dan River basin polarity stratigraphy (Fig. S4), the normal-reverse couplet seen in the Cumnock is most simply correlated to polarity chron E8 of the Newark-APTS (Figs. S3 and S4), although there is a thin but well-defined (in terms of demagnetization behavior) reverse polarity interval in samples 187.70, 192.02, and 194.65 m (615.8, 630.0, and 638.6 ft). This reverse zone is most simply correlated to the reverse polarity zone at the base of CH-C-1-81. The two thin reverse zones were not observed in E8n in the Princeton core, which may be due to much lower temporal resolution and/or continuity in those fluvial sediments.

Based on this correlation (Fig. S3), the Cumnock Formation comprises only two 405-ky cycles, the period of which corresponds to the cycle thickness of 82.1 m (Fig. S3). The accumulation rate of the lower member of the Cow Branch based on this correlation is 0.312 m/ky. When this accumulation rate is multiplied by the ratio between the Cumnock and lower Cow Branch formations the accumulation rate for the Cumnock Formation is 0.219 m/ky.

Assuming this average accumulation rate for the Cumnock, data on rock color have periods of 3.8, 4.3, and 24.3 m that correspond in time to periods of 17.4, 19.6, and 110.0 ky, respectively, which match well the predicted period of the two modal precessional periods and the short eccentricity cycle. Less well-defined peaks exist at 2.8 m (12.8 ky) and 7.3 m (33.3 ky).

Periods indistinguishable from those in the rock color data are observed in the portion of the core we sampled for $\delta^{13}C_{org}$ (Fig. 3 in the main text and Dataset S1, *B*), although, because this is a subsample, all of the peaks are more spread out. TOC concentration variations are nearly identical to the color periods. $\delta^{13}C_{org}$ values tend to be more enriched in ^{13}C in the deeper-water, more organic-rich units and more ^{13}C-depleted in the organic-poor units, following the pattern seen in the Lockatong Formation of the Newark basin (13, 14), typical of broad rifts of eastern North America where the enhanced efficacy of the biological pump during deep-water times overwhelmed other effects. Fourier analysis of the $\delta^{13}C_{org}$ data indicates a strong shift toward the 24.3-m (111.0-ky) cycle and as much power at the semiprecessional period 2.2 m (10.1 ky) as at the precessional periods around 4.2 m (19.2 ky) (Fig. 3 in the main text). Interestingly, both rock color and the geochemical data have periods very similar to those seen in Fourier analysis of gamma ray data from the Butler no. 1 exploration well described by Hu and Textoris (10).

Based on available paleomagnetic data (Fig. S3), the Cumnock Formation was deposited beginning at 226 Ma at the equator. Traversodonts are known from the shallow water facies of the Cumnock Formation (15, 16), the underlying Pekin Formation (16), and the overlying Sanford Formation (17) in the Sanford subbasin as well as from Lithofacies association II the Durham basin (18). Extrapolating from the correlation to the Newark-APTS, Fig. S3 and biostratigraphic correlation (19), the upper Pekin Formation was deposited at 2°S latitude at approximately 231 Ma. The youngest traversodont-producing strata in the Sanford subbasin are in the lower Sanford Formation, deposited at approximately 1°N latitude at approximately 224 Ma. The traversodonts from Lithofacies Association II in the Durham subbasin are the same age as the middle Sanford Formation of the Sanford subbasin and were deposited at approximately 3°N at 222 Ma (20). In total, the Deep River basin traversodont-bearing strata were deposited in a 5° swath around the Triassic paleoequator, over at least a 9-My interval, during which time the climate responded to the semiprecessional cycle.

Solite Quarry, Upper Member of the Cow Branch Formation, Dan River Basin. The Cow Branch Formation of the Dan River (Danville) basin is a thick, (+2 km) cyclical gray and black lacustrine unit comprised of two members informally termed the lower and upper members (Figs. S1, S3, and S4). A very rich aquatic assemblage has been recovered from this formation (21, 22), and the paleomagnetic reversal stratigraphy of the basin section is known in more detail than any other southern basin (12) (Fig. S4). As yet, no traversodonts or procolophonids are known from this basin; however, there has been no prospecting in the more terrestrial strata in which they would be expected. The lacustrine

strata do show the strongest semiprecessional cyclicity of all units in this study (Fig. S1).

The lacustrine record of the upper member of the Cow Branch Formation is best displayed in the three quarries of the former Virginia Solite Corporation in Leaksville Junction, North Carolina. We measured depth ranks for all three quarry sections and computed their fast Fourier transform (FFT) power spectra (Fig. S4 and Table S1). All three sections have significant periods in their spectra at around 46, 11, and 6 m that are highly coherent (Fig. S4). By correlating the magnetic polarity stratigraphy of the Dan River basin with the Newark basin time scale, we determined an average accumulation rate for the Solite sections of 0.463 m/ky (Fig. S4). Using this accumulation rate, the main periods in the Solite depth rank sections are roughly 100, 24, and 13 ky (Figs. S1 and S4). In addition, section 2 is just long enough to begin to have resolvable power at 405 ky (175 m, 378 ky). Field mapping confirms that the sedimentary expression of the 400-ky cycle is a prominent part of the Dan River section in general (12).

The Dan River basin lacustrine record thus shares with the Newark basin periodic lake level cycles of roughly 400, 100, and 20 ky. The characteristic two peaks that average approximately 100 ky are also present, as seen in the Newark basin power spectra (Fig. S1). However, unlike the Newark basin record, the most prominent cycles in all three Dan River basin sections are of 10- to 15-ky duration. Visual examination of the Solite quarry outcrops reveals that well-developed cycles comparable to those attributed to the approximately 20-ky cycles in the Newark basin are present, and these correspond to the approximately 20-ky cycles seen in the power spectra (Fig. 3 in the main text). However, each of these cycles tends to have two deep-water intervals, rather than just one as seen in the Newark basin. The two deep-water intervals are responsible for the approximately 10-ky peaks in the power spectra.

We analyzed 15 samples of the uppermost two cycles in section 2 of the Solite Quarry for $\delta^{13}C_{org}$. The upper cycle produces the lagerstätten described in refs. 21 and 22 (Fig. S3 and Dataset S1, *B*). Sampling density amounted to about 1 sample/0.6 m or 1 sample/1,600 y, using our age model. These samples had been collected in the early 1980s and analyzed for TOC, carbonate, and sulfur at that time (23). Both cycles preserve a pattern comparable to that seen in the narrow rift basins of eastern North America, with relatively negative values in the deeper water units and relatively more positive values in the shallow water units. This pattern differs from that seen in the Cumnock Formation in which the more important process for the isotopic ratios of organic matter seems to have been the efficacy of the biological pump (Fig. S1). As expected from the Fourier analysis of depth ranks, there are two zones of relative negative values per cycle due to preferential preservation of lignin-derived organic matter in the shallow water units. We note that the Dan River basin, at least as presently preserved, is the narrowest of all the exposed rift basins (Fig. 1 in the main text), and the strata were deposited at a paleolatitude of 4° (Fig. 1 in the main text) (24).

Nursery No. 1 Core, Lockatong Formation, Newark Basin. Newark basin cyclicity has been understood in broad outline for almost half a century (25), and nearly the entire cyclostratigraphy has been recovered in core and described (5, 6, 11). For this study we selected the middle Lockatong Formation from about the middle of the Byram Member to the middle of the Skunk Hollow Member in the Nursery no. 1 core (Fig. S1). Based on magnetostratigraphic polarity correlation (Fig. S4), we analyzed depth ranks from the interval that is directly contemporaneous with section 2 of the Solite Quarry section (Dataset S1, *B*). The most prominent period is at 4.6 m corresponding to the 20-ky cycle, and there are two other strong periods at 20 m (90 ky) and 100 m (approximately 400 ky) based on the FFT consistent with the results of Olsen and Kent (26). Although there is a minor period at 2.8 m (12 ky), it is obvious that there is far less of a semiprecession signal in the Lockatong compared to the Solite sections. The paleolatitude of Nursery no. 1 core is 7° (Fig. 1 in the main text) (27).

Andrus no. 1 and Lenn Bros. no. 1 cores, Balls Bluff Formation, Culpeper basin. We examined two cores from the largely red Balls Bluff Formation of the Culpeper basin recording depth ranks and color (Dataset S1, *B*). The two cores stratigraphically overlap with an unambiguous cyclostratigraphic correlation (Fig. S1) and were reported on briefly and figured with the polarity stratigraphy by Olsen and Kent (27). Correlation with the Newark basin section is straightforward. The paleolatitude of these cores was 13° N (Fig. 1 in the main text). Based on correlation to the Newark-APTS, the accumulation rate averages 0.2225 m/ky. The prominent thickness periods at 18.7 ky (4.2 m), 22.0 ky (4.9 m), and 23.4 ky (5.2 m) represent climatic precession, the periods at 86.7 ky (19.3 m) and 112.3 ky (25.0 m) represent short eccentricity, and the cycle at 380.6 ky (84.7 m) is the 405-ky long eccentricity cycle. Other prominent thickness periods at 7.3 and 11.4 m may be smeared-out 20-ky cycles, although similar periods occur in the Nursery core. There are only hints of semiprecessional periods at approximately 12.5 ky (2.8 m), similar to the Nursery core. The paleolatitude of this sequence is 12°N.

Somerset no. 1 Core, Passaic Formation, Newark Basin. This core (Fig. S1) was studied as part of the original series of papers on the Newark basin coring project (e.g., refs. 11 and 26), and the FFT of this specific part of the Nursery core (Dataset S1, *B*) is closely comparable to that of the contemporaneous Andrus and Lenn Bros. cores. Here we use the Newark-APTS the same way we did for the latter and calculate an average accumulation rate of 0.1647 m/ky. The untuned spectrum of this part of the Somerset core has prominent periods at 21.6 ky (3.6 m), 26.4 ky (4.4 m), 108.8 ky (17.9 m), and 411.2 ky (67.7 m). As in the Andrus and Lenn Bros. cores, there is a hint of semiprecession at approximately 12 ky (2.0 m). Kent and Tauxe (24) corrected the paleolatitudes originally determined for the Newark basin cores (11) for inclination error, and this forms the basis of all the paleolatitudes used here, extrapolated from the time-space nomogram of Fig. 1 in the main text. Consequently, the paleolatitude for this part of the Somerset core is 15°N.

Methods and Background for Insolation Model. At the equator, the sun passes overhead twice a year, once at the vernal equinox ($\lambda = 0$) and once at the autumnal equinox ($\lambda = \pi$). This leads to two potential times of maximum daily insolation during the year, and a complementary twice yearly minimum daily insolation at the summer solstice ($\lambda = \pi/2$) and winter solstice ($\lambda = 3\pi/2$).

Daily solar insolation averaged over 24 h at latitude φ and day λ (rad, independent of calendar date) is given by (28, 29)

$$W = (S_0/\pi) \cdot [1 + e\cos(\lambda\text{-}\omega\text{-}\pi)]^2/(1-e^2)^2 \cdot (H_0 \sin\varphi \sin\delta + \cos\varphi \cos\delta \sin H_0), \quad \textbf{[S1]}$$

where S_0 is the solar constant (1,365 W/m^2), H_0 is the hour angle, and δ is the declination angle. The orbital parameters of eccentricity e, obliquity ε, and precession ω are given by Laskar et al. (30) (abbreviated below as La2004) and provide

$$\sin\delta = \sin\varepsilon \sin\lambda, \quad \textbf{[S2]}$$

$$\cos H_0 = -\tan\varphi \tan\delta. \quad \textbf{[S3]}$$

Eq. **S1** can be simplified for the equatorial case (31–33):

$$W_{eq} = (S_0/\pi) \cdot [1 + e\cos(\lambda \cdot \omega \cdot \pi)]^2/(1-e^2)^2 \cdot \cos\delta. \quad \textbf{[S4]}$$

As shown by Ashkenazy and Gildor (33), because $e \ll 1$ and $\sin(\varepsilon) \approx \varepsilon$, Eq. **S4** can be approximated by

$$W_{eq} \approx (S_0/\pi(1-e^2)^2) \cdot \left(1 - 2e\cos(\lambda \cdot \omega) - \frac{1}{2}\varepsilon^2 \sin^2 \lambda\right). \quad \textbf{[S5]}$$

Earth's precession (ω) dictates which equinox receives greater daily insolation at the equator each year. As shown by Berger et al. (32), if we assume eccentricity (e) and obliquity (ε) constant over an approximately 21–ky precession period, then

Vernal equinox ($\lambda = 0$) is maximum for $\pi/2 \le \omega \le 3\pi/2$

Autumnal equinox ($\lambda = \pi$) is maximum for $3\pi/2 \le \omega \le 2\pi$, $0 \le \omega \le \pi/2$

Summer solstice ($\lambda = \pi/2$) is minimum for $0 \le \omega \le \pi$

Winter solstice ($\lambda = 3\pi/2$) is minimum for $\pi \le \omega \le 2\pi$. **[S6]**

Precession has an approximately 21-ky cycle, and so the maxima (and minima) switch between the equinoxes (and the solstices) twice every 21 ky. This can be seen as an approximately 11-ky cycle in the spectral analysis of maximum and minimum equatorial insolation (see figure 4c and d in ref. 33). As illustrated by Eq. **6**, switching between equinoxes and switching between solstices as the insolation extremes is out of phase by $\pi/2$ in the precessional index. Therefore, one of the two extremes switches seasons approximately every 5 ky, as can be seen by the 5-ky cycle in the spectral analysis of maximum-minimum insolation (figure 5 in ref. 32). The approximately 100-ky and approximately 405-ky cycles are also observed in the spectral analyses due to the modulation of equatorial insolation by eccentricity.

Maximum and minimum insolation do not always occur precisely on the equinoxes and solstices. The roots of differentiating Eq. **5** with respect to $\lambda(\delta W_{eq}/\delta\lambda = 0)$ gives a better approximation of the days (λ, in rad) of maximum and minimum insolation. Let the expected days of maxima (equinoxes, $\lambda = 0$ and $\lambda = \pi$) and minima (solstices, $\lambda = \pi/2$ and $\lambda = 3\pi/2$) be called λ_e and the approximated days of maxima and minima be called λ_a. Then, using the approximations given by Ashkenazy and Gildor (33),

$$\cos\lambda_e \approx \cos\lambda_e - \sin\lambda_e(\lambda_a \cdot \lambda_e) \quad \textbf{[S7]}$$

$$\sin\lambda_e \approx \sin\lambda_e + \cos\lambda_e(\lambda_a \cdot \lambda_e), \quad \textbf{[S8]}$$

a solution for the days of maxima and minima insolation is found to be (33)

$$\lambda_0 = \sin\omega/[(-\varepsilon 2/2e) + \cos\omega] \quad \text{for } \lambda \approx 0 \quad \textbf{[S9]}$$

$$\lambda_\pi = \sin\omega/[(\varepsilon 2/2e) + \cos\omega] + \pi \quad \text{for } \lambda \approx \pi \quad \textbf{[S10]}$$

$$\lambda_{\pi/2} = -\cos\omega/[(\varepsilon 2/2e) + \sin\omega] + \pi/2 \quad \text{for } \lambda \approx \pi/2 \quad \textbf{[S11]}$$

$$\lambda_{3\pi/2} = -\cos\omega/[(-\varepsilon 2/2e) + \sin\omega] - \pi/2 \quad \text{for } \lambda \approx 3\pi/2. \quad \textbf{[S12]}$$

These adjustments to the timing of insolation extremes do not reduce the strength of the approximately 11-ky cycle, and they have been shown to enhance the strength of the eccentricity cycles seen in frequency analysis (see figure 4 in ref. 33).

Moving away from the equator, the timing of insolation extremes, λ, vary with increasing magnitude. To find the magnitude and day of maximum and minimum insolation at nonequatorial latitude φ, we use a MATLAB program that implements Eq. **1** and the La2004 orbital parameter solution (see below and Dataset S1, *D*). The program iteratively calculates daily solar insolation for $\lambda\max \pm d$ rad and $\lambda\min \pm d$ rad with steps of 0.02 rad, where $\lambda\max$ and $\lambda\min$ are the equinoxes and solstices, respectively. For $\varphi < 10°$, $d = 0.8$ is sufficient. For $\varphi > 10°$, d must increase with φ.

Because of chaotic diffusion of planetary orbital motions and uncertainties in initial condition, the La2004 solution for the orbital parameters is not reliable beyond 50–60 Ma. However, the 405-ky eccentricity cycle is more stable than the others and deviates by only two periods by 250 Ma (30), and the frequencies of approximately 20 ky, approximately 40 ky, approximately 100 ky, and approximately 405 ky have been observed in cyclic sedimentary sequences through the Phanerozoic (34, 35). Although differences from Cenozoic values are to be expected in deep time, we find it reasonable to use the La2004 solution in these calculations to characterize the cyclicity in low-latitude insolation during the Late Triassic because the basic geometry problem will not have changed.

Matlab Script (See Dataset S1, *D*).

```
%This program inputs values of eccentricity, obliquity and
%precession angle to calculate annual maximum and minimum insolation at a
%given latitude.  To call this function, type MMInsol(latDeg) into the
Matlab command prompt,
%replacing the term "latDeg" with the latitude, in degrees, at which you
%want to calculate maximum and minimum annual insolation.

%To run this program, you must use a text file containing the following
%information in columns:
   %Time in kyr at 0.1 kyr intervals
   %the Laskar 2004 solution to Eccentricity for the correct time range
   %the Laskar 2004 solution to Obliquity (in radians) for the correct time range
   %the Laskar 2004 solution to Precession Angle (in radians) for the
   %correct time range

% A text file containing this information for the past 100kyr is provided
% along with this program. The text file is called
Dataset_S4_Orb_param.xlsx
% same as a text file and rename it Orb_param.txt
% Information in this text file was obtained from the Laskar's
% downloadable program at
% http://www.imcce.fr/Equipes/ASD/insola/earth/earth.html
% This program can be used to download similar information for periods of
% time other than the past 100kyr. To use newly downloaded information,
```

```
% put it into a text file in the proper order, and rename it Orb_param.

% Citation for Laskar's downloadable program:

%A&A 428, 261-285 (2004), DOI: 10.1051/0004-6361:20041335
%Laskar, J., Robutel, P., Joutel, F., Gastineau, M., Correia, A.C.M.,
Levrard, B. : 2004,
%A long term numerical solution for the insolation quantities of the Earth.

%%%%%%%%%%%%%%%%%%%%%%%%%%%%%%%%%%%%%%%%%%%%%%%%%%%%%%%%%%%%%%%%%%%%%%%%%%%%%%%

% If you use this program, please cite:
% PNAS (2011)
% Whiteside, J.H., Grogan, D.S., Olsen, P.E., Kent, D.V. Climatically driven
% biogeographic provinces of Late Triassic tropical Pangea


latDeg=0;  %Set this parameter to equal the latitude, in degrees, at which
to calculate insolation


load Orb_param.txt;
Time=Orb_param(:,1); %Time is in kyr bp at 0.1 kyr intervals, time bp is
negative
Eccen=Orb_param(:,2);
Obliq=Orb_param(:,3);
Prec=Orb_param(:,4);


S=1365;    %S=solar constant := 1350 W/m^2
Pi=3.141592654;
K=S/Pi;


Lambda=0:.02:6.2; %Lambda is the longitude of the Earth in radians
lat=latDeg*(Pi/180); %change latitude in degrees to latitude in radians

for k=1:310;
   %calculate insolation for all lambda values, 0 to 2Pi at steps of .02
   Del(:,k)=asin(sin(Obliq).*sin(Lambda(1,k)));
   H(:,k)=acos(-tan(lat).*tan(Del(:,k)));

z(:,k)=H(:,k).*sin(lat).*sin(Del(:,k))+cos(lat).*cos(Del(:,k)).*sin(H(:,k));
   Cos(:,k)=cos(Lambda(1,k)-Prec-Pi);
   Denom=(1-Eccen.^2).^2;

   Insol(:,k)=(S/Pi)*z(:,k).*((1+Eccen.*Cos(:,k)).^2)./Denom;

end


%find the minimum insolation
for k=1:length(Insol);
    MinInsol(k,1)=min(Insol(k,:));
  for j=1:310
     if min(Insol(k,:))==Insol(k,j)
        MinInsol(k,2)=(0+.02*j)*(180/Pi); %This is the Earth longitude
in degrees that corresponds to the time of min insolation
     end
  end
end

%find maximum insolation

plot(Time, MinInsol)

for k=1:length(Insol);
    RowB(k,:)=Insol(k,:);
    MaxInsol(k,1)=max(RowB(k,:));
  for j=1:310
     if max(RowB(k,:))==RowB(k,j)
        MaxInsol(k,2)=(0+.02*j)*(180/Pi); %This is the Earth longitude
in degrees that corresponds to the time of max insolation
```

```
    end
  end
end

Table(:,1)=MinInsol(:,1);
Table(:,2)=MinInsol(:,2);
Table(:,3)=MaxInsol(:,1);
Table(:,4)=MaxInsol(:,2);
Table(:,5)=Time;

figure;plot(Time,MinInsol(:,1),Time,MaxInsol(:,1))



%To compare this solution to potential maximum and minimum solutions at
the
%solstices and equinoxes, uncomment the below calculations and plots:

%Lambda = 0 is the vernal equinox
%Lambda = Pi is the autumnal equinox
%Lambda = Pi/2 is the summer solstice
%Lambda = 3Pi/2 is the winter solstice

%name all variables same as above, but with _new to differentiate


%Uncomment below for loop to calculate insolation at equinoxes and
solstices:

Lambda_new=[0,Pi,Pi/2,3*Pi/2];

for k=1:4;
  Del_new(:,k)=asin(sin(Obliq).*sin(Lambda_new(1,k)));
  H_new(:,k)=acos(-tan(lat).*tan(Del_new(:,k)));

z_new(:,k)=H_new(:,k).*sin(lat).*sin(Del_new(:,k))+cos(lat).*cos(Del_new(:
,k)).*sin(H_new(:,k));
  Cos_new(:,k)=cos(Lambda_new(1,k)-Prec-Pi);
  Denom_new=(1-Eccen.^2).^2;


Insol_new(:,k)=(S/Pi)*z_new(:,k).*((1+Eccen.*Cos_new(:,k)).^2)./Denom_new;
end


%the first column of Insol_new is insolation at Lambda = 0
%the second column of Insol_new is insolation at Lambda = Pi
%the third column of Insol_new is insolation at Lambda = Pi/2
%the fourth column of Insol_new is insolation at Lambda = 3Pi/2




%Uncommend any of the plots below to view

%To plot the equinoxes against MaxInsol (recommended for low lat):
%figure;plot(Time,Insol_new(:,1),Time,Insol_new(:,2),Time,MaxInsol(:,1))

%To plot solstices against MinInsol (recommended for low lat):
%figure;plot(Time, Insol_new(:,3),Time,Insol_new(:,4),Time,MinInsol(:,1))

%To plot the equinoxes against MinInsol (recommended for high lat):
%figure;plot(Time,Insol_new(:,1),Time,Insol_new(:,2),Time,MinInsol(:,1))

%To plot solstices against MaxInsol (recommended for high lat):
%figure;plot(Time, Insol_new(:,3),Time,Insol_new(:,4),Time,MaxInsol(:,1))
```

Phylogeny and Nitrogen Excretion. We reconstructed the ancestral states of nitrogen secretion for procolophonids and traversodonts using squared-change parsimony in Mesquite v.2.5 (36) (Fig. S5). Two ancestral state reconstructions of the excretory physiology of amniotes were examined: with turtles as archosauromorph diapsids (e.g., refs. 37 and 38) or nested within parareptiles (e.g., refs. 39 and 40). With either alternative, traversodont cynodonts are unequivocally urea excreters. With turtles as parareptiles, procolophonids are unambiguous uric acid excreters. With turtles within Diapsida the character state is ambiguous, but it is a reasonable hypothesis that parareptiles would have uric acid excretion, as do all living sauropsids. Backbone phylogeny follows refs. 41–43 for basal amniotes, and refs. 44–46 for synapsids.

1. Sues H-D, Olsen PE (1990) Triassic vertebrates of Gondwana aspect from the Richmond basin of Virginia. *Science* 249:1020–1023.
2. Sues H-D, Hopson JA (2010) Anatomy and phylogenetic relationships of *Boreogomphodon jeffersoni* (Cynodontia: Gomphodontia) from the Upper Triassic of Virginia. *J Vertebr Paleontol* 30:1202–1220.
3. LeTourneau PM (1999) Depositional history and tectonic evolution of Late Triassic age rifts of the US Central Atlantic margin: Results of an integrated stratigraphic, structural, and paleomagnetic analysis of the Taylorsville and Richmond basins. PhD thesis (Columbia Univ, New York).
4. Cornet B (1993) Applications and limitations of palynology in age, climatic and paleoenvironmental analyzes of Triassic sequences in North America. *New Mexico Mus Nat Hist Sci Bull* 3:75–93.
5. Olsen PE, Kent DV (1999) Long-period Milankovitch cycles from the Late Triassic and Early Jurassic of eastern North America and their implications for the calibration of the early Mesozoic time scale and the long-term behavior of the planets. *Philos Trans R Soc A* 357:1761–1787.
6. Olsen, PE, Kent DV, Whiteside JH (2011) Implications of the Newark Supergroup-based astrochronology and geomagnetic polarity time scale (Newark-APTS) for the tempo and mode of the early diversification of the Dinosauria. *Earth Environ Sci Trans R Soc Edinburgh* (in press).
7. Malinconico MAL (2002) Lacustrine organic sedimentation, organic metamorphism and thermal history of selected Early Mesozoic Newark Supergroup basins, Eastern USA. PhD thesis (Columbia Univ, New York).
8. Ediger VS (1986) Paleopalynological biostratigraphy, organic matter deposition and basin analysis of the Triassic-(?)Jurassic Richmond rift basin, Virginia, USA. PhD thesis (Pennsylvania State Univ, State College, PA).
9. Olsen PE, et al. (1989) Field guide to the tectonics, stratigraphy, sedimentology, and paleontology of the Newark Supergroup, eastern North America. *International Geological Congress, Guidebooks for Field Trips* T351 (American Geophysical Union, Washington, DC).
10. Hu LN, Textoris DA (1994) Cycles in lake beds of the Triassic Sanford Sub-basin of North Carolina. *SEPM Concepts in Sedimentology and Paleontology* (Society for Sedimentary Geology, Tulsa, OK) Vol 4, pp 5–23.
11. Kent DV, Olsen PE, Witte WK (1995) Late Triassic-Early Jurassic geomagnetic polarity and paleolatitudes from drill cores in the Newark rift basin (Eastern North America). *J Geophys Res* 100:14965–14998.
12. Kent DV, Olsen PE (1997) Magnetostratigraphy and paleopoles from the Late Triassic Dan River-Danville basin: Interbasin correlation of continental sediments and a test of the tectonic coherence of Newark rift basins in eastern North America. *Geol Soc Am Bull* 109:366–377.
13. Whiteside JH (2006) Catastrophic, climatic, and biotic modulation of ecosystem evolution. PhD thesis (Columbia Univ, New York).
14. Whiteside JH, et al. (2011) Pangean great lake paleoecology on the cusp of the end-Triassic extinction. *Palaeogeogr Palaeoclimat Palaeoecol* 301:1–17.
15. Heckert AB, Schneider V, Olsen PE, Nesbitt S (2006) A new microvertebrate fauna from the upper Triassic (Norian) Cumnock Formation, Durham Subbasin, North Carolina, USA. *Geol Soc Am Abstracts with Programs* 38:23. Available at http://gsa.confex.com/gsa/2006SE/finalprogram/abstract_101756.htm.
16. Heckert AB, Schneider VP, Olsen PE, Mitchell JS (2009) Vertebrate diversity of the Upper Triassic Chatham Group, Deep River basin, central North Carolina. *Abstracts, Second Annual Meeting of the Southeastern Association of Vertebrate Paleontology* Virginia Museum of Natural History, Martinsville, VA), p 8. Available at http://web.me.com/dooleyclan/SEAVP/SEAVP_files/Abstract%20book.pdf.
17. Olsen PE, Schneider V, Sues H-D, Peyer KM, Carter JG (2001) Biotic provinciality of the Late Triassic equatorial humid zone. *Geol Soc Am Abstracts with Programs* 33:A-27. Available at http://gsa.confex.com/gsa/2001SE/finalprogram/abstract_4541.htm.
18. Sues H-D, Olsen PE, Carter JG (1999) A Late Triassic traversodont cynodont from the Newark Supergroup of North Carolina. *J Vertebr Paleontol* 19:351–354.
19. Lucas SG, Huber P (2003) Vertebrate biostratigraphy and biochronology of the nonmarine Late Triassic. *The Great Rift Valleys of Pangea in Eastern North America. Sedimentology, Stratigraphy, and Paleontology,* eds LeTourneau PM, Olsen PE (Columbia Univ Press, New York) Vol 2, pp 143–191.
20. Olsen PE, Huber P (1997) Stop 3: Triangle Brick Quarry. *TRIBI: Triassic Basin Initiative, Abstracts with Programs and Field Trip Guidebook*, ed Clark TW (Duke Univ, Durham, NC) pp 22–29.
21. Olsen PE, Remington CL, Cornet B, Thomson KS (1978) Cyclic change in Late Triassic lacustrine communities. *Science* 201:729–733.
22. Fraser NC, Grimaldi DA, Olsen PE, Axsmith B (1996) A Triassic Lagerstâtte from Eastern North America. *Nature* 380:615–619.
23. Olsen PE (1984) Comparative paleolimnology of the Newark Supergroup: A study of ecosystem evolution. PhD thesis (Yale Univ, New Haven, CT).
24. Kent DV, Tauxe L (2005) Corrected Late Triassic latitudes for continents adjacent to the North Atlantic. *Science* 307:240–244.
25. Van Houten FB (1962) Cyclic sedimentation and the origin of analcime-rich upper Triassic Lockatong Formation, west-central New Jersey and adjacent Pennsylvania. *Am J Sci* 260:561–576.
26. Olsen PE, Kent DV (1996) Milankovitch climate forcing in the tropics of Pangea during the Late Triassic. *Palaeogeogr Palaeoclimat Palaeoecol* 122:1–26.
27. Olsen PE, Kent DV (2000) High resolution early Mesozoic Pangean climatic transect in lacustrine environments. *Zentralbl Geol Palaontol*, VIII:1475–1496.
28. Milankovitch M (1941) *Kanon der Erdbestrahlung und seine Andwendung auf das Eiszeitenproblem* (Royal Serbian Academy of Sciences, Belgrade).
29. Berger A (1978) Long-term variations of daily insolation and Quaternary climatic changes. *J Atmos Sci*35:2362–2367.
30. Laskar J, et al. (2004) A long-term numerical solution for the insolation quantities of the Earth. *Astron Astrophys* 428:261–285.
31. Berger A, Loutre MF (1997) Intertropical latitudes and precessional and half-precessional cycles. *Science* 278:1476–1478.
32. Berger A, Loutre MF, Mélice JL (2006) Equatorial insolation: From precession harmonics to eccentricity frequencies. *Clim Past* 2:131–136. Available at http://www.clim-past.net/2/131/2006/cp-2-131-2006.html.
33. Ashkenazy Y, Gildor H (2008) Timing and significance of maximum and minimum equatorial insolation. *Paleoceangraphy* 23:PA1206, 10.1029/2007PA001436.
34. Olsen PE (1986) A 40-million-year lake record of early Mesozoic orbital climatic forcing. *Science* 234:842–848.
35. Meyers SR.(2008) Resolving Milankovitchian controversies: the Triassic Latemar limestone and the Eocene Green River formation. *Geology* 36:319–322.
36. Maddison WP, Maddison DR (2008) Mesquite: A modular system for evolutionary analysis, Version 2.5. Available at http://mesquiteproject.org.
37. Hedges SB, Poling LL (1999) A molecular phylogeny of reptiles. *Science* 283:998–1001.
38. Bhullar B-AS, Bever GS (2009) An archosaur-like laterosphenoid in early turtles (Reptilia: Pantestudines). *Breviora* 518:1–11.
39. Reisz RR, Laurin M (1991) *Owenetta* and the origin of turtles. *Nature* 349:324–326.
40. Lyson TR, Bever GS, Bhullar B-AS, Joyce WG, Gauthier JA (2010) Transitional fossils and the origin of turtles. *Biol Lett* 6:830–833
41. Gauthier J, Kluge AG, Rowe T (1988) Amniote phylogeny and the importance of fossils. *Cladistics* 4:105–209.
42. Laurin M, Reisz RR (1995) A reevaluation of early amniote phylogeny. *Zool J Linn Soc* 113:165–223.
43. Reisz RR (1997) The origin and early evolutionary history of amniotes. *Trends Ecol Evol* 12:218–222.
44. Sidor CA, Hopson JA (1998) Ghost lineages and "mammalness": assessing the temporal pattern of character acquisition in the Synapsida. *Paleobiology* 24:254–273.
45. Rubidge BS, Sidor CA (2001) Evolutionary patterns among Permo-Triassic therapsids. *Annu Rev Ecol Syst* 32:449–480.
46. Luo Z-X (2007) Transformation and diversification in mammal evolution. *Nature* 450:1011–1019.

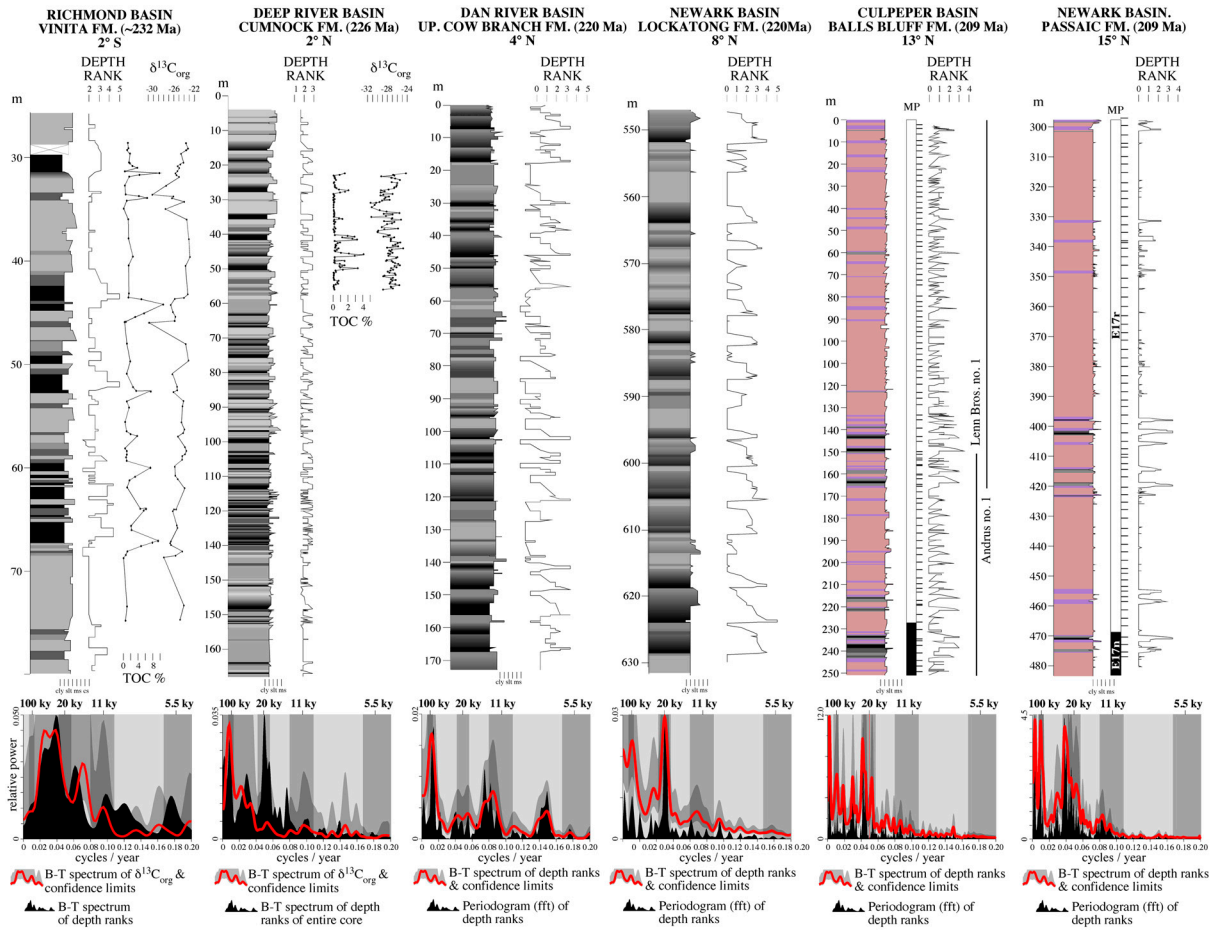

Fig. S1. Main lacustrine sections analyzed with their frequency spectra. Colors in the sections are representative of, although shown here more saturated than, the actual rock color. MP, magnetic polarity (black is normal, white reverse); B-T, Blackman–Tukey spectrum.

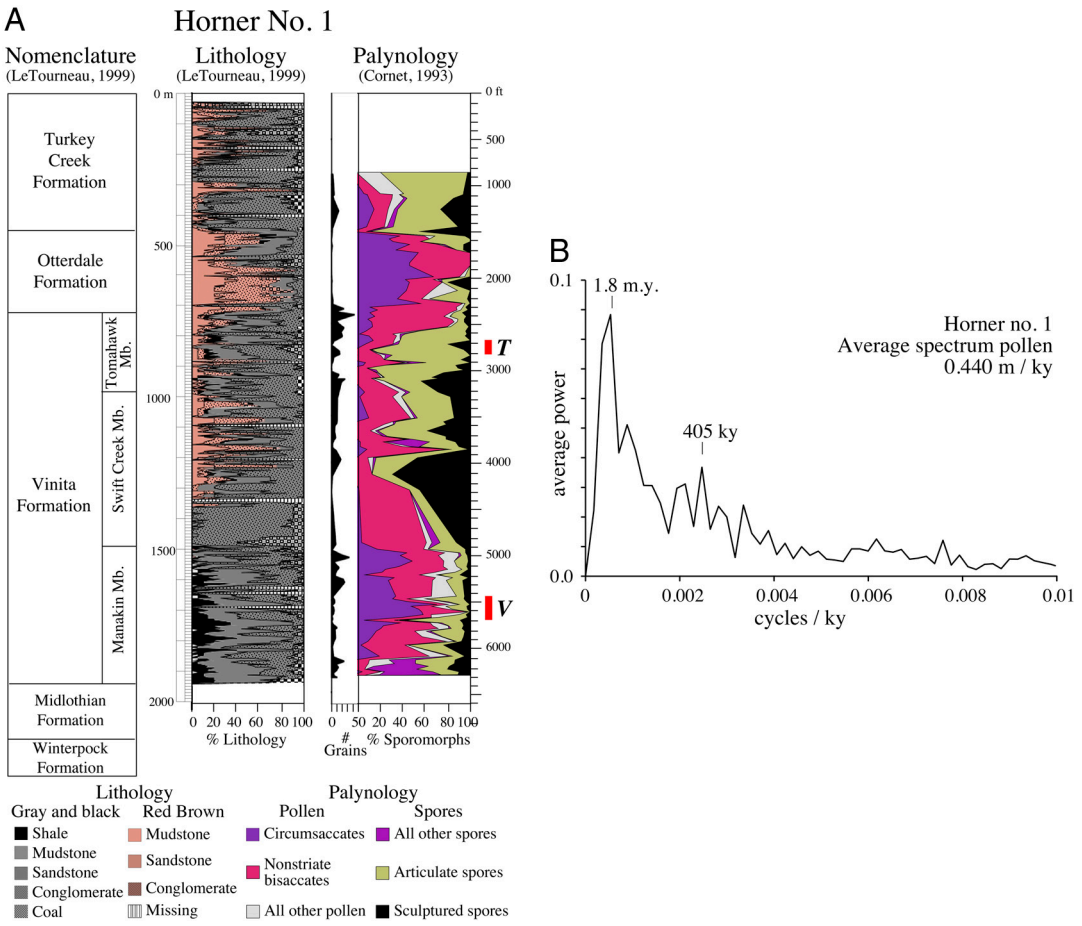

Fig. S2. (*A*) Lithology and sporomorph data from the Horner no. 1 well in the Richmond basin from refs. 3 and 4. Red bars show the projected position of the Vago no. 1 core (**V**) and traversodonts (Table S1) (**T**). (*B*) Average of spectra of pollen morphotypes shown in Fig. S2. Peak at 0.00560 m/cycle is set at 405 ky.

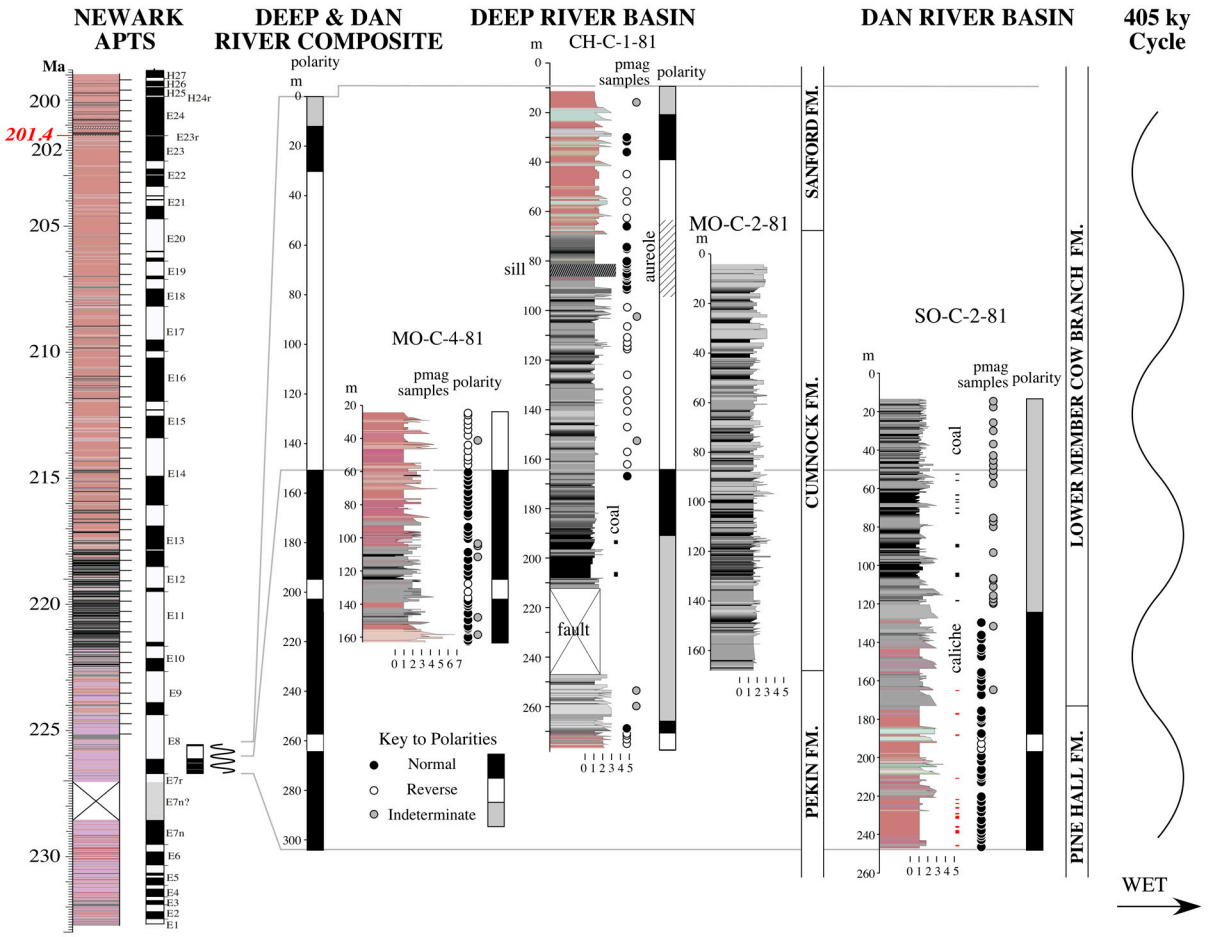

Fig. S3. Correlation between the Cumnock Formation of the Deep River basin in Cores MO-C-4-81, MO-C-4-81, and CH-C-1-81, the lower member of the Cow Branch in core SO-C-2-81 and the Newark-APTS.

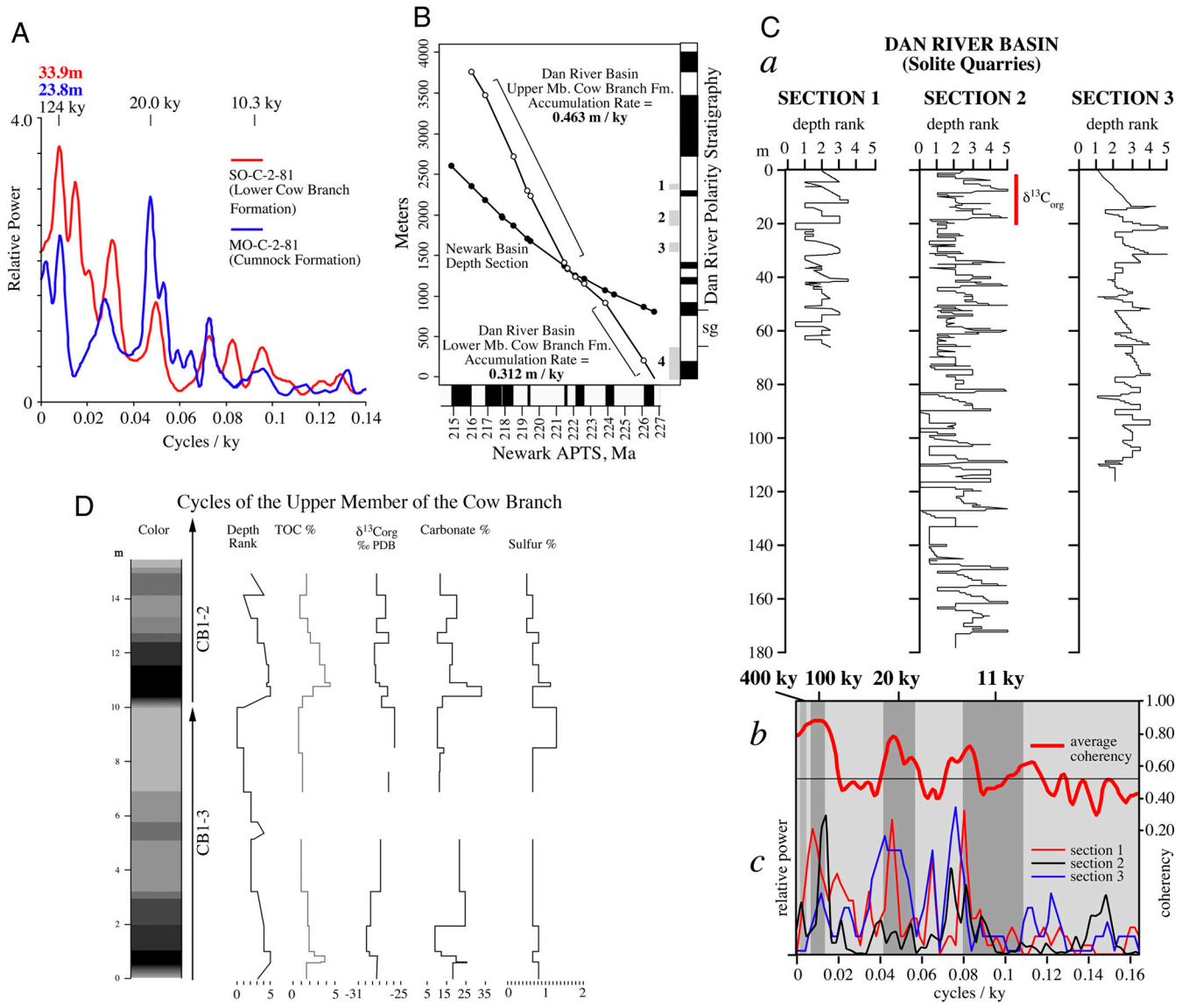

Fig. S4. (*A*) Blackman–Tukey spectra of Cumnock and lower Member of the Cow Branch Formation. (*B*) Correlation between the Newark-APTS and the Dan River section (gray bars 1, 2, and 3 show the positions of Solite Quarry sections 1, 2, and 3; gray bar 4 is the lower member of the Cumnock Formations as seen in core SO-C-2-81 in Fig. S3. "sg" is position of a gap in sampling of outcrop and core). (*C*) Data from the upper member of the Cow Branch Formation of the Dan River basin at the Solite quarry. [(*a*) Depth ranked sections from the three Solite quarry sections; red bar labeled $\delta^{13}C$ is section of 2 cycles shown in *D* (depth ranks increase in value with interpreted lake depth; see ref. 26). (*b*) Coherency between all three Solite sections (see Table S1 for locations); coherencies above the horizontal line are significant at the >95% level; all three pairwise coherency analyses were performed and the results averaged; (*c*) FFTs of all three sections. Note the consistent set of peaks between 12 and 8 ky.] (*D*) Detailed geochemical and depth rank data from the uppermost two cycles in section 2 of the Solite Quarry (see *C*) that correspond to cycles CB1-3 and CB1-2 described in ref. 21. CB1-2 is the source of the main lagerstätte described in refs. 21 and 22 (carbon, sulfur, and carbonate data are from ref. 23).

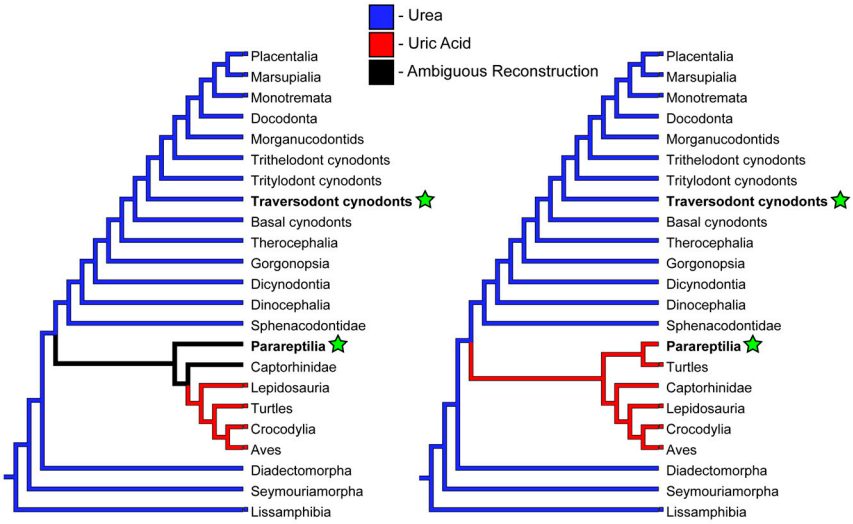

Fig. S5. Ancestral state reconstruction of the excretory physiology of amniotes with alternate phylogenetic hypotheses based on the position of turtles as diapsids or nested within parareptiles (see *SI Text*). The two extinct taxa of interest, traversodont cynodonts and parareptiles, are highlighted by green stars.

Table S1. Metadata for cores and sections

Core or section	Formation	Age	Age, Ma	N Latitude	W Longitude
Vago no. *	Vinita	Carnian	approximately 230–235	37.60333	77.69111
Horner no. 1 †	Vinita, Otterdale	Carnian	approximately 230–235	37.451178	77.740343 †
MO-C-2-81 ‡	Cumnock	E. Norian	226	35.451944	79.384722
CH-C-1-81 ‡	Cumnock	E. Norian	226	35.558333	79.215000
MO-C-4-81 ‡	Cumnock	E. Norian	226	35.334722	79.466111
SO-C-2-81 ‡	lower Cow Branch	E. Norian	226	36.286389	80.140833
Solite Quarry 1	upper Cow Branch	E. Norian	220	36.543739	79.675194
Solite Quarry 2	upper Cow Branch	E. Norian	220	36.539083	79.671929
Solite Quarry 3	upper Cow Branch	E. Norian	220	36.538088	79.664241
Nursery no. 1 §	Lockatong	E. Norian	220	40.289594	74.823437 ¶
Lenn no. 1 ‖	Balls Bluff	L. Norian	209	38.460657	77.906449
Andrus no. 1 ‖	Balls Bluff	L. Norian	209	38.462522	77.923172
Somerset no. 1 §	Passaic	L. Norian	209	40.505763	74.565385 **

*Virginia Department of Mines, Minerals, and Energy Division of Geology and Mineral Resources, Charlottesville, VA.
†Lamont-Doherty Earth Observatory, Eastern United States onshore repository.
‡North Carolina Geological Survey, Raleigh Field Office and Repository, Raleigh, NC.
§Rutgers/New Jersey Geological Survey Rift-Drift Core Repository, Piscataway, NJ.
¶Nursery location given as 40° 18′ 03″N, 74° 49′ 27″W in refs 1 and 2, corrected here.
‖US Geological Survey Herndon Warehouse.
**Somerset location given as 40° 30′ 31″N, 74° 33′ 58″W in Table S2: Metadata for traversodont and procolophonid specimens.

1 Kent DV, Olsen PE (1999) Astronomically tuned geomagnetic polarity time scale for the Late Triassic. *J Geophys Res* 104:12831–12841.
2 Olsen PE, Kent DV, Cornet B, Witte WK, Schlische RW (1996) High-resolution stratigraphy of the Newark rift basin (Early Mesozoic, Eastern North America). *Geol Soc Am* 108:40–77.

Table S2. Metadata for traversodont and procolophonid specimens

Taxon and species no. (T = traversodont P = procolophonid)	Basin	Formation	Age, Ma	N Latitude	W Longitude
cf. *Hypsognathus* (P) [a]	Dunbarton	unnamed	approximately 211	33.1348	81.3549
Boreogomphodon jeffersoni (T) 21371 [b c]	Deep River	Pekin	approximately 231	35.637730	78.996560
Traversodontia sp. (T) 24722 [b]	Deep River	Cumnock	225	35.597481	79.017703
Traversodontia sp. (T) 25570 [b]	Deep River	Sanford	223	35.574844	79.015673
Boreogomphodon herpetairus (T) 15576 [d]	Durham	Lithofacies association II	approximately 220	35.871660	78.898939
Boreogomphodon jeffersoni (T) 448632[e]	Richmond	Vinita	approximately 233	37.462504	77.672058
Gomphiosauridion baileyae, (P) 448630 [e]	Richmond	Vinita	approximately 233	37.462504	77.672058
cf. *Hypsognathus* (P) [f]	Newark	Passaic	215	40.579146	75.080242
Hypsognathus fenneri (P) VP-2160[g]	Newark	Passaic	210	40.416325	75.514066
Hypsognathus fenneri (P) 1676 [h]	Newark	Passaic	208	40.862694	74.141998
Hypsognathus fenneri (P) 11643 [e]	Newark	Passaic	202	40.893738	74.168146
Hypsognathus fenneri (P) [i]	Newark	Passaic	202	40.308980	75.834927
Hypsognathus fenneri (P) 55831[j]	Hartford	New Haven	approximately 203	41.543594	72.822859
Arctotraversodon plemmyridon (T) 990GF89.1 [k]	Fundy	Wolfville	approximately 233	45.316	63.782
Acadiella psalidodon (P) 19190 [l]	Fundy	Wolfville	approximately 233	45.137537	64.324608
Haligonia bolodon (P) 996GF74.1 [k]	Fundy	Wolfville	approximately 233	45.311538	63.806942
Scoloparia glyphanodon (P) 996GF83.1 [k]	Fundy	Wolfville	approximately 233	45.145533	64.273762
Hypsognathus cf. *fenneri* (P) 998GF45.1 [k]	Fundy	Blomidon	215	45.193205	64.358524

[a]Core from Savannah River Plant Deep Rock Boring number 11 (SRP DRB-11) at 641.4 m (2,015.7 ft) archived at the Savannah River Site.
[b]North Carolina Museum of Natural Sciences, Raleigh, NC.
[c]Fig. 2 *Upper Left* in the main text.
[d]Department of Geology, University of North Carolina, Chapel Hill, NC.
[e]United States National Museum, Washington, DC.
[f]Private collection of Jack Boyland.
[g]State Museum of Pennsylvania, Harrisburg, PA.
[h]American Museum of Natural History, New York, NY.
[i]Reading Public Museum, Reading, PA (specimens).
[j]Yale Peabody Museum, New Haven, CT (specimen found in rubble rock wall).
[k]Nova Scotia Museum, Halifax, NS, Canada.
[l]Yale Peabody Museum, New Haven, CT (Princeton Collection).

Other Supporting Information Files

Dataset S1 (XLS)